TBMCE 2022

5th International Conference on

TECHNOLOGIES & BUSINESS MODELS FOR CIRCULAR ECONOMY

CONFERENCE PROCEEDINGS

Sanja **POTRČ**

Miloš **BOGATAJ**

Zdravko **KRAVANJA**

Zorka **NOVAK PINTARIČ**

EDITORS

University of Maribor Press

University of Maribor

Faculty of Chemistry and Chemical Engineering

5th International Conference on Technologies & Business Models for Circular Economy

Conference Proceedings

Editors

Sanja Potrč

Miloš Bogataj

Zdravko Kravanja

Zorka Novak Pintarič

January 2023

Title
Naslov
5th International Conference on Technologies & Business Models for Circular Economy

Subtitle
Podnaslov
Conference Proceedings

Editors
Uredniki
Sanja Potrč
(University of Maribor, Faculty of Chemistry and Chemical Engineering)

Miloš Bogataj
(University of Maribor, Faculty of Chemistry and Chemical Engineering)

Zdravko Kravanja
(University of Maribor, Faculty of Chemistry and Chemical Engineering)

Zorka Novak Pintarič
(University of Maribor, Faculty of Chemistry and Chemical Engineering)

Technical editor
Tehnični urednik
Jan Perša
(University of Maribor, University Press)

Cover designer
Oblikovanje ovitka
Jan Perša
(University of Maribor, University Press)

Graphic material
Grafične priloge
Authors of proceedings & editors

Conference
Konferenca
TBMCE, International Conference on Technologies & Business Models for Circular Economy

Date and location
Datum in kraj
September 12th to September 14th 2022, Portorož, Slovenia

Published by / *Založnik*
University of Maribor
University Press
Slomškov trg 15, 2000 Maribor, Slovenija
https://press.um.si, zalozba@um.si

Issued by / *Izdajatelj*
University of Maribor
Faculty of Chemistry and Chemical Engineering
Smetanova ulica 17, 2000 Maribor, Slovenija
https://www.fkkt.um.si/, fkkt@um.si

Publication type / *Vrsta publikacije*
E-book

Edition / *Izdaja*
1st

Available at / *Dostopno na*
http://press.um.si/index.php/ump/catalog/book/748

Published at / *Izdano*
Maribor, January 2023

REPUBLIKA SLOVENIJA
MINISTRSTVO ZA GOSPODARSKI RAZVOJ IN TEHNOLOGIJO

REPUBLIC OF SLOVENIA
MINISTRY OF ECONOMIC DEVELOPMENT AND TECHNOLOGY

"Častni pokrovitelj dogodka je bil g. Matjaž Han, minister za gospodarski razvoj in tehnologijo."

"The event was under the honorary patronage of Mr. Matjaž Han, Minister of Economic Development and Technology."

Gospodarska zbornica Slovenije
Združenje kemijske industrije

REPUBLIKA SLOVENIJA
SLUŽBA VLADE REPUBLIKE SLOVENIJE ZA RAZVOJ IN EVROPSKO KOHEZIJSKO POLITIKO

surovina

muflon

Saubermacher Slovenija

mikropolo
YOUR PARTNER IN THE LABORATORY

CINKARNA

Radenska ADRIATIC

IKEMA d.o.o.
INŠTITUT ZA KEMIJO, EKOLOGIJO, MERITVE IN ANALITIKO
www.ikema.si

IOS Inštitut za okoljevarstvo in senzorje

SPIRIT SLOVENIJA

Financira Evropska unija
NextGenerationEU

CIP - Kataložni zapis o publikaciji
Univerzitetna knjižnica Maribor

330:502.131.1(082)(0.034.2)

INTERNATIONAL Conference on Technologies & Business Models for Circular Economy (5 ; 2022 ; Portorož)
5th International Conference on Technologies & Business Models for Circular Economy [Elektronski vir] : conference proceedings : [September 12th to September 14th 2022, Portorož, Slovenia] / editors Sanja Potrč ... [et al.]. - 1st ed. - E-zbornik. - Maribor : University of Maribor, University Press, 2023

Način dostopa (URL): https://press.um.si/index.php/ump/catalog/book/748
ISBN 978-961-286-692-1 (PDF)
doi: 10.18690/um.fkkt.1.2023
COBISS.SI-ID 139091459

ISBN 978-961-286-692-1 (pdf)

DOI https://doi.org/10.18690/um.fkkt.1.2023

Price
Cena Free copie

For publisher
Odgovorna oseba založnika Prof. Dr. Zdravko Kačič,
Rector of University of Maribor

Attribution
Citiranje Potrč, S., Bogataj, M., Kravanja, Z., Novak Pintarič, Z., (eds.). (2023). 5th *International Conference on Technologies & Business Models for Circular Economy* Maribor: University Press. doi: 10.18690/um.fkkt.1.2023

University of Maribor Press

Table of Contents

Dog Rose Oil Extract as a Potential Green Corrosion Inhibitor 1
Regina Fuchs-Godec

Microwave Irradiation of Alkali-activated Metakaolin Slurry 9
Barbara Horvat, Branka Mušič, Majda Pavlin,Vilma Ducman

Pilot Production of Façade Panels: Variability of Mix Design 25
Majda Pavlin, Barbara Horvat, Vilma Ducman

Recyclability of Recycled Concrete Products in Cements 45
Santiago Rosado, Lidia Gullón, Leticia Presa, Jaime Moreno

Catalyzed Degradation of Polyethylene Terephthalate 53
Žiga Samsa, Darja Pečar, Andreja Goršek

Electrocoagulation Implementation for Textile Wastewater Treatment Processes 61
Marjana Simonič

Dog Rose Oil Extract as a Potential Green Corrosion Inhibitor

Regina Fuchs-Godec
University of Maribor, Faculty of Chemistry and Chemical Engineering, Maribor, Slovenia
regina.fuchs@um.si

Abstract The inhibitory effect of the hydrophobic layer on the surface of copper in an acidic medium was studied by the classical potentiodynamic method and the impedance spectroscopy method. The hydrophobic character of the copper surface was achieved by immersing the sample in ethanolic octadecanoic acid with and without the addition of dog rose oil extract. The selected concentrations of the added dog rose oil extract were 0.5, 1.0, and 2.0 wt% in 0.05 molL-1 alcoholic solution of octadecanoic acid. Based on electrochemical measurements, an inhibition effect of ≈ 65% was obtained when the surface was modified by immersion in ethanolic octadecanoic acid only. With the addition of dog rose oil extract, this value increased to over 90%, depending on the concentration of dog rose oil extract added.

Keywords:
copper,
green corrosion inhibitor,
dog rose oil extract,
acid corrosion,
EIS

University of Maribor Press

DOI https://doi.org/10.18690/um.fkkt.1.2023.1
ISBN 978-961-286-692-1

1 Introduction

The existence of industry and related industrial processes is inconceivable without metallic materials. Despite all progress and research in the field of corrosion, it is still not possible to completely stop the deterioration of metallic materials by degrading corrosion reactions. By using various protective coatings, inhibitors acting through adsorption mechanisms, and intelligent materials, we can only slow down the corrosion processes more or less effectively. Progress has been made, but it is still far from complete success. More recently, "green orientation' and the circular economy have been added, prescribing both environmental protection and the sensible use and handling of raw materials and zero-waste production in the sense of 'every waste can be a raw material' (Abbasi, 2019) In other words: Products (food supplements) that have passed their expiration date can also be included in this group, but this expiration date is not necessarily mandatory in all areas. (Fuchs-Godec, 2021) (Patil, 2021). The hydrophobic properties of metals and alloys with high surface energy have recently attracted much attention from both researchers and academia, mainly because of their great importance in daily life and in various industrial and biological applications.

The present work focuses on the study of the inhibition properties of a dog rose oil extract added to the alcoholic solution of a fatty acid at a concentration of c = 50 mmol/L to form a self-assembled hydrophobic layer on the surface of copper. The selected concentrations of the added oil extract were 0.5, 1.0, and 2.0 wt%. Two electrochemical methods were used for the corrosion studies, namely a classical potentiodynamic method (PD) and electrochemical impedance spectroscopy (EIS). Measurements were performed in an acidic medium (acid rain), varying the pH (pH = 1, 3 and 5).

2 Experimental

For polarisation measurements, we chose a classical three-electrode system and a Tacussel type CEC/TH polarisation cell with a thermostatic sheath. All potentials were measured against an Ag/AgCl (3M KCl) reference electrode. The counter electrode was platinum and the working electrode was copper (99.9%).

The surface area of the sample affected by the test solution was approximately 0.875 cm^2. Polarisation curves were recorded from -0.4 V to a maximum of 0.3 V versus Ag/AgCl. The potential increased continuously at a scanning rate of 1 mVs^{-1}. Polarisation curves were recorded 30 minutes after sample immersion (stabilisation of the sample at the open circuit potential OCP occurred for 30 minutes). All measurements were performed at a temperature of 25°C ± 1°C. For the potentiodynamic and impedance measurements, we used a potentiostat/galvanostat/ZRA-Gamry Reference 600™ with the associated software to analyse the measurements.

Before etching, the metal surface was successively abraded using a grinding machine and SiC papers of grades 800, 1000, 1200 and 2400. Etching was performed in aqueous solutions of 10% HNO_3 for 1 minute and then washed in deionized water and dried with compressed air.

Subsequently, the etched sheets were immersed at room temperature for about two hours in a 50 mmol/L ethanolic solution of octadecanoic acid with and without the addition of various concentrations of dog rose oil extract.

3 Results and discussions

The polarization curves in Figure 1 show the voltage-current response of the untreated and modified copper surfaces in a simulated acid rain solution with different pH values = 5, 3, and 1. The surfaces of the copper samples were modified by immersion in an alcoholic solution of octadecanoic acid with and without the addition of the dog rose oil extract at different concentrations (0.5, 1.0, and 2.0 wt%).

Considering the untreated surface, significant changes are observed in both the cathodic and anodic regions. The cathodic and anodic current density decreases. In the case where the surface of Cu was modified in the mixture with added dogrose oil extract, its values decrease by almost three orders of magnitude in all selected corrosion media. This is particularly effective in the most aggressive medium, namely in the case where the pH of the corrosion medium was pH = 1. In this case, the surface protection is significantly lower when the protective hydrophobic coating consists only of octadecanoic acid. The corrosion current density is only slightly

lower than the corrosion current density of the untreated surface. However, the corrosion current density decreases by two orders of magnitude when the dog rose oil extract is added at all three selected concentrations. The decreasing trend is from the lowest concentration chosen to the highest.

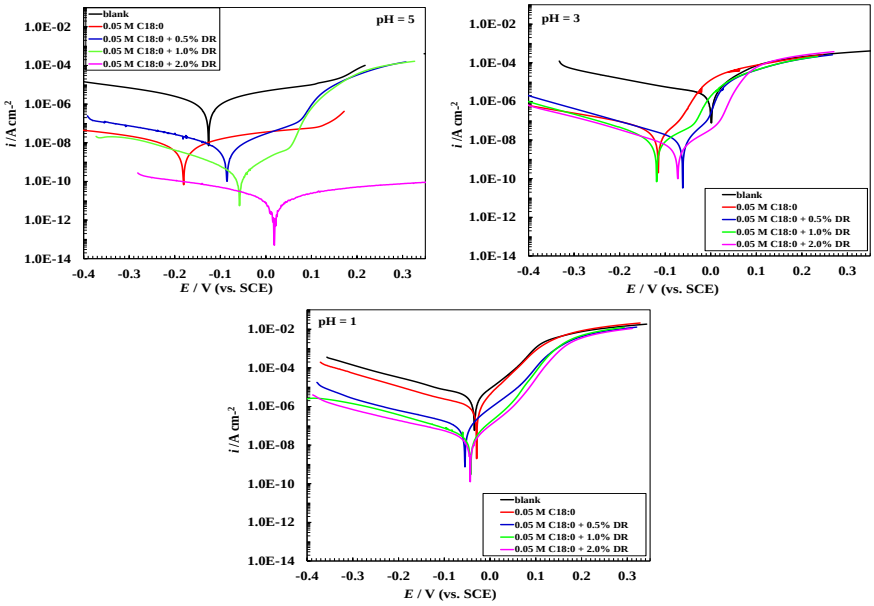

Figure 1: Potentiodynamic polarisation curves (1 mVs^{-1}) of Cu for the bare and modified surfaces of the 'acid rain' solutions (pH =5, 3 and 1) at 25°C. The modified surface was prepared by the immersion of the sample in 0.05 M alcoholic solution of octadecanoic acid with and without the addition of dogrose (DR).

Source: own.

Table 1: The inhibition efficiency η determined based on the kinetic parameters for the corrosion of Cu from the potentiodynamic polarisation curves for the bare and modified surfaces of the 'acid rain' solutions (pH =5, 3 and 1) at 25°C. The modified surfaces were prepared by immersing Cu in 0.05 M stearic acid in ethanol with and without the addition of Dog Rose (DR).

Corrosive media acid rain, pH = 5	wt% DR	% η_{icorr}	% η_{Rp}
modified surface of Cu	**0***	97.8	97.4
	0.5	98.5	98.7
	1.0	99.3	99.4
	2.0	99.7	99.8

Corrosive media acid rain, pH = 3	wt% DR	% η_{icorr}	% η_{Rp}
modified surface of Cu	**0***	95.2	94.1
	0.5	97.5	97.7
	1.0	99.5	99.6
	2.0	99.8	99.8

Corrosive media acid rain, pH = 1	wt% DR	% η_{icorr}	% η_{Rp}
modified surface of Cu	0*	65.2	66.4
	0.5	92.3	93.1
	1.0	98.0	96.4
	2.0	99.1	99.2

The inhibition efficiency η was calculated via the kinetic parameters measured during corrosion processes, as well as the polarisation resistance R_p, the corrosion current density i_{corr}, In the case of the polarisation resistance, η was calculated via Equation (2), where while Equation (1) was used in connection with the corrosion current density (Table 1).

$$\eta\% = \left[1 - \frac{i'_{corr}}{i_{corr}}\right] \cdot 100 \quad (1)$$

$$\eta\% = \left[1 - \frac{R_p}{R_p{}'}\right] \cdot 100, \quad (2)$$

where the notations i_{corr}, R_p, were used for those measurements without inhibition action, whilst the primed quantities i_{corr}', R_p' were applied when measurements were performed on the modified surfaces of copper in simulated solution of acid rain with pH = 1, 3 or 5.

The Nyquist diagrams confirm the results of the potentiodynamic measurements. In the case of the unprotected surface, depressed semicircles appear at all selected pH values of the corrosion medium, followed by a straight line with a slope of about 45◦ in the low-frequency region, indicating diffusion processes in the formed oxide layer of the untreated copper sample. As expected, this is least pronounced when the pH of the corrosion medium is 5 and most pronounced at pH=1. The diffusion tail does not appear at pH=5 in the case of the surface modified with both octadecanoic acid

alone and with the addition of dog rose oil extract. In the case of 2% addition of DR, a polarisation resistance of 12.5 MΩcm2 is obtained, which places the resulting self-assembled layer among the stable layers.

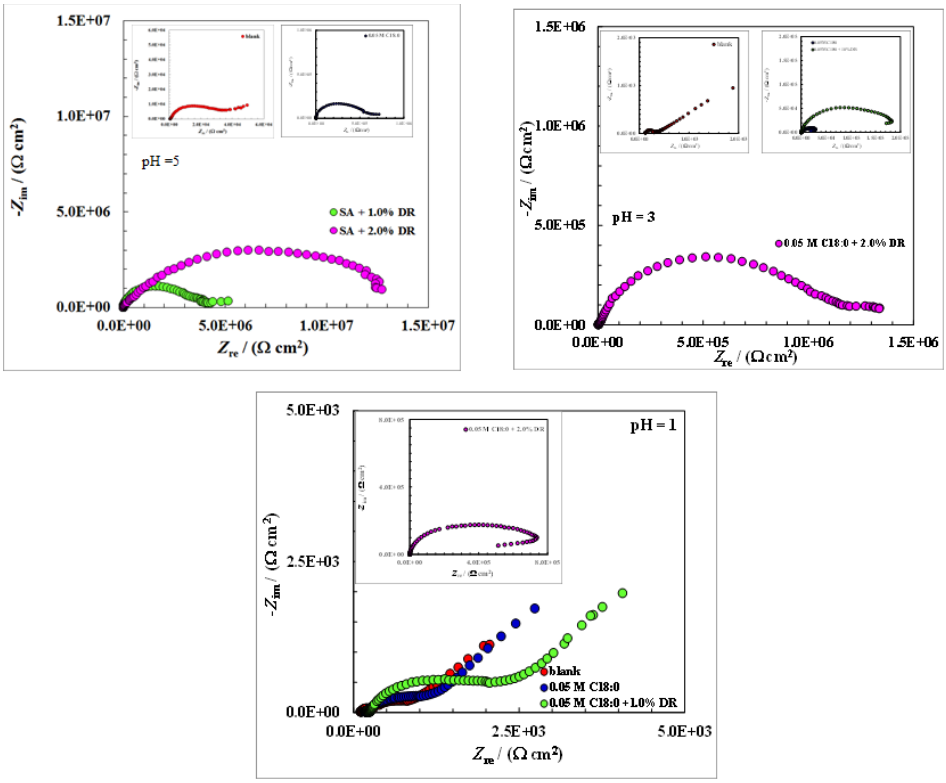

Figure 2: Nyquist diagrams of Cu for the bare and modified surfaces in the 'acid rain' solutions (pH =5, 3 and 1) at 25°C.

Source: own.

Acknowledgments

This work was financially supported by Slovenian Research Agency under research project "Physico-Chemical Processes on the Surface Layers and Application of Nanoparticles" (P2-0006).

References

Abbasi, S., Nouri, M., Sabour Rouhaghdam, A. (2019). A novel combined method for fabrication of stable corrosion resistance superhydrophobic surface on Al alloy. *Corrosion Science, 159,* 108144 doi.org/10.1016/j.corsci.2019.108144

Fuchs-Godec, R. (2021). A Synergistic Effect between Stearic Acid and (+)-α-Tocopherol as a Green Inhibitor on Ferritic Stainless Steel Corrosion Inhibition in 3.0% NaCl Solution. Coatings, 11, 8, 971. doi.org/10.3390/coatings11080971

Patil, C.K., Jung, D.W., Jirimali, H.D., Baik, J.H., Gite, V.V., Hong, S.C. (2021). Nonedible Vegetable Oil-Based Polyols in Anticorrosive and Antimicrobial Polyurethane Coatings. *Polymers*, *13*, 3149. doi.org/10.3390/ polym13183149

Microwave Irradiation of Alkali-activated Metakaolin Slurry

Barbara Horvat, Branka Mušič, Majda Pavlin, Vilma Ducman

Slovenian National Building and Civil Engineering Institute, Ljubljana, Slovenia
barbara.horvat@zag.si, branka.music@zag.si, majda.pavlin@zag.si, vilma.ducman@zag.si

Abstract The building and civil engineering industry generates more than 40% of man-caused carbon emissions, consumes a lot of energy just to produce building materials, generates a large amount of waste through construction and demolition, and consumes a large amount of natural resources. One of the possible solutions is to use alkali-activated materials, which can use waste instead of raw materials and are produced at lower temperatures, with less energy consumption and in less time than traditional building products. All of this lowers the carbon footprint, which could be further reduced by the timely-short implementation of microwave irradiation in the early stages of alkali-activation synthesis. Therefore, metakaolin activated with Na-water glass in a theoretically optimal ratio was irradiated with microwaves of 2.45 GHz at powers of 100 W and 1000 W for 1 min, and compared to non-irradiated reference cured only at room conditions. Samples prepared at higher power, i.e., 1000 W, solidified completely and foamed. TG-DTA was performed on all samples in the early stages of curing, mechanical strengths were measured on 3 and 28-day-old samples, and leaching tests on aged samples.

Keywords: alkali-activation, metakaolin, microwaves, TG/DTA, mechanical strengths

University of Maribor Press

DOI https://doi.org/10.18690/um.fkkt.1.2023.2
ISBN 978-961-286-692-1

1 Introduction

Alkali-activated materials (AAMs) are made from solid pulverized precursors containing a significant amount of amorphous Si and Al "activated" by alkali (hydroxides or/and silicate solution) (Provis, 2013). The process of alkali-activation starts with the dissolution of the precursor in the alkali liquid, rearrangement of the dissolved components into monomers with help of diffusion, followed by the "coagulation" of the monomers into the dehydrated polymer (Marvila et al., 2021; Pacheco-Torgal et al., 2008). This inorganic polymer consists of SiO_2 and AlO_2^{1-} tetrahedra connected through O-bridges, where the 1^- charge of Al is compensated by ions of the 1st and 2nd group of the periodic system (Škvára, 2007). The formed aluminosilicate network (ASN) is usually and mainly amorphous, and when the precursor used is metakaolin, the AAM can also be called a geopolymer (Ameri et al., 2019).

If compact ASN is foamed, AAM becomes alkali-activated foam (AAF), i.e., a lightweight material with lower geometric density, lower mechanical strength, but higher acoustic and/or thermal insulation ability. The foaming process can be mechanical (Hajimohammadi et al., 2017a), chemical (Burkhard Walther et al., 2017; Hajimohammadi et al., 2017b) and/or physical (Fletcher et al., 2005; Horvat and Ducman, 2020a; Rincón Romero et al., 2019; Wei et al., 2016). The mechanical introduction of the pores into the alkali-activated slurry of proper viscosity (not too low, otherwise bubbles would escape, and not too high, since reaching a uniform distribution of the pores could not be achieved) is done by mechanical mixing of the pre-prepared foam with the freshly alkali-activated slurry, in which the chemical reactions are still in progress. Chemical foaming (Horvat and Ducman, 2019) is performed by adding foaming agents (e.g., liquid H_2O_2, solid Na-perborate, solid pulverized Al) and stabilizing agents (e.g., liquid triton, solid soybean lecithin, solid Na-oleate, solid Na-dodecyl sulphate) to the solid pulverized precursor or to the liquid alkali. Solid ingredients are mixed with the solid precursor and liquid ingredients are mixed with the liquid alkali to avoid premature reactions and loss of bubbles. Homogenized solids and homogenized liquids are mixed as briefly as necessary to ensure wetting of the components and uniform distribution of all reagents. Besides induced chemical foaming, self-foaming (Horvat and Ducman, 2020b) may occur if the precursor contains substances that react with alkali(s) with

the release of gasses into the slurry, ending as alkali-activated self-foam (AAsF). Foaming reactions can be immediate (AAF) or delayed (AAdF), as also some precursors require less time for curing (metakaolin, slags) and others more (fly-ash, mineral wools) if curing is performed under room conditions. If the curing temperature is increased, the curing time is reduced (Horvat and Ducman, 2019) and the release of bubbles out from the slurry is hindered.

In this work, the influence of irradiation with microwaves of different power on alkali-activated metakaolin slurry in its early stages was studied. Metakaolin was used for alkali-activation because this material is widely used in alkali-activated research.

2 Method

For chemical (X-ray fluorescence, XRF; Thermo Scientific ARL Perform'X Sequential XRF) and mineralogical (X-ray powder diffraction, XRD; Empyrean PANalytical X-ray Diffractometer, Cu X-Ray source) analysis of metakaolin (MK), the precursor was dried, milled and sieved below 125 μm.

XRF measurement was performed on molten discs and analysed using UniQuant 5. The XRD diffractogram was solved using X'Pert Highscore plus 4.1. Rietveld refinement was performed with an external standard (corundum, Al_2O_3) to estimate the amount of amorphous content and minerals.

From the XRF and XRD results, the amounts of Si, Al and 1st group of the periodic system were determined as described in our previous work (Horvat and Ducman, 2019). The amount of substance of precursor and added alkali (Na-silicate solution, Geosil, 344/7, Woelner, Ludwigshafen, Germany, 16.9% Na_2O, 27.5% SiO_2) for Si, Al, Na was aimed to be 1.9, 1, "≤1", respectively, to achieve the highest possible compressive strength and avoid efflorescence (Duxson et al., 2005). The theoretically determined mass ratio between precursor and Na-silicate solution was 1:0.66, respectively.

After mixing MK with alkali until the slurry was completely wetted, the slurry was moulded into moulds made of silicone-urethane rubber. Reference was cured exclusively under room conditions, while the others were irradiated with microwaves

of frequency 2.45 GHz, with power of 100 W and 1000 W, for 1 min, not-covered and covered with another silicone-urethane rubber mould to avoid rapid dehydration while the sample was being irradiated. The inverter type microwave (Panasonic, NN-CD575M) was used, i.e., the microwaves work constantly, unlike an ordinary kitchen microwave where the microwaves work for a short period of time, then turn off and repeat the cycle.

The mechanical strengths (bending and compressive) of the AAMs were measured with a compressive and bending strength testing machine (ToniTechnik ToniNORM) 3 and 28 days after moulding.

Thermogravimetric analysis and differential thermal analysis (TG/DTA; STA 409 PC Luxx, Netzsch, Germany) were performed on all samples 12 min after mixing the ingredients and compared with the non-irradiated sample more than 1-year-old. Fresh samples were followed to constant mass. Samples of about 40 mg were heated in airflow from room temperature to 1000 °C at a rate of 10 K/min to evaluate the mass changes (mainly water losses) as a function of temperature.

Moisture of the 3 and 28-day-old samples was determined by mass loss using an IR moisture analyser (Mettler Toledo, HE73).

Evaluation of the presence of toxic elements in leachates was performed on 28-day-old samples according to the European standard SIST EN 12457-2. AAM/AAF was crushed to grain sizes lower than 4 mm and added into deionised water in a glass bottle with solid:liquid mass ratio of 1:10, respectively. Suspensions were rotated around the vertical axis for 24 h at room conditions, then filtered below 0.45 μm. The obtained liquid fraction was acidified to pH<2 with HNO_3 for determination of the amount of released metals by inductively coupled plasma mass spectrometer (ICP-MS, Agilent 7900). Results were compared to the total amount of toxic trace and minor elements measured in the precursor and with the legislation (Decre on waste landfill).

3 Results

Chemical analysis (XRF) of MK is shown in Table 1. Regarding the potential for use as a precursor in alkali-activation, MK contains a significant amount of SiO_2 and Al_2O_3 needed for ASN formation, while elements of the 1st and 2nd group are scarce, allowing the possibility of adding more alkali and still avoiding efflorescence.

Table 1: Oxides with mass percent (m%) above 0.1% present in MK according to XRF analysis.

Oxides [m%]	Na_2O	K_2O	MgO	CaO	Al_2O_3	SiO_2	TiO_2	Fe_2O_3
XRF	0.29	0.18	0.17	0.48	25.58	69.46	1.13	2.32

The XRD diffractogram of MK (Figure 1, black line) shows the presence of the amorphous content (the amorphous halo has 2θ peak around 25°, indicating that the Si:Al ratio is above 2:1 (Tokoro et al., 2014), which is consistent with the XRF results in Table 1) and minerals, where quartz represents the majority. Mineralogical analysis of MK with Rietveld refinement, presented in Table 2, shows more than 60% of the amorphous content and more than 30% of quartz.

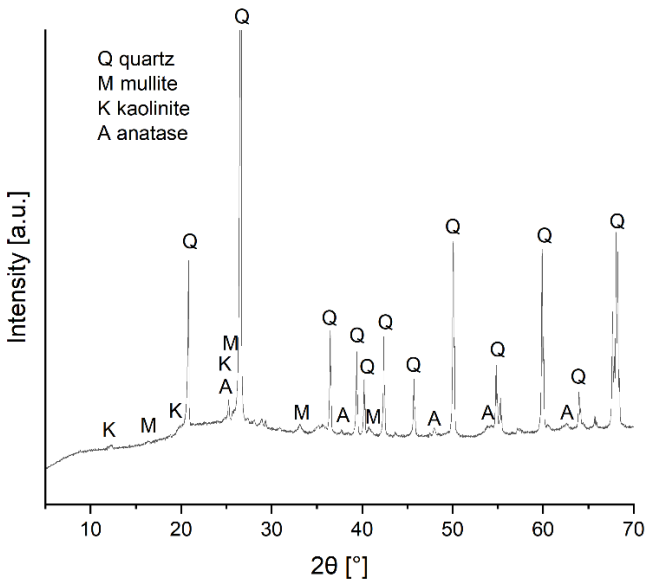

Figure 1. XRD pattern of MK.

Source: own.

Table 2. Minerals in mass percent (m%) present in MK according to Rietveld refinement analysis on XRD pattern.

Minerals [m%]	Quartz	Mullite	Kaolinite	Anatase	Amorphous content
XRD	33.5	3.3	1.1	0.5	61.6

The XRF (Table 1) and XRD (Table 2) results were recalculated onto elements to estimate the amount of amorphous content per element (Table 3) (Horvat and Ducman, 2019).

Table 3. Mass percentage of elements in the amorphous content.

Elements [m%]	Na	K	Mg	Ca	Al	Si
XRF-XRD	0.21	0.15	0.10	0.35	11.96	16.21

The amount of amorphous content of Si:Al in the mixture of MK and Na-silicate solution together was aimed to be 1.9:1, respectively. The mass ratio of MK and Na-silicate solution, 1:0.66, resulted in the amount of substance ratios Si:Al:1st group:2nd group=1.99:1:0.84:0.03. If not all (amorphous) Al dissolves, efflorescence still might not occur, since the initial amount of substance of alkali ions is below Al.

The visual results of alkali-activation are shown in Figure 2. Irradiation of freshly moulded alkali-activated MK slurry with microwaves at 100 W for 1 min (Figure 2, (b) samples 2 and 3) resulted in AAM looking like non-irradiated AAM (Figure 2, (b), sample 1). While irradiation with microwaves at 1000 W for 1 min caused alkali-activated slurry to foam (Figure 2, (b), samples 4 and 5) and the material hardened completely, which was in comparison with other samples very hot immediately after irradiation. If the mould was sealed when the slurry was irradiated at 1000 W (Figure 2, (c), samples 5 and 6), and if the slurry "touched" the cover during foaming (Figure 2, (c), sample 6), it began to damage material's framework from above. This can be seen on the top surface in Figure 2, (c), sample 6, and its' side surface in Figure 2, (d).

The thermal behaviour of the samples was determined by TG/DTA, and is shown in Figure 3, Figure 4 and Table 4: 1-year-old non-irradiated sample (red), fresh non-irradiated sample (orange), irradiated sample at 100 W for 1 min (light blue), irradiated sample at 100 W for 1 min and covered during microwave irradiation (dark

blue), irradiated sample at 1000 W for 1 min (light pink), and irradiated sample at 1000 W for 1 min and covered during microwave irradiation (dark pink).

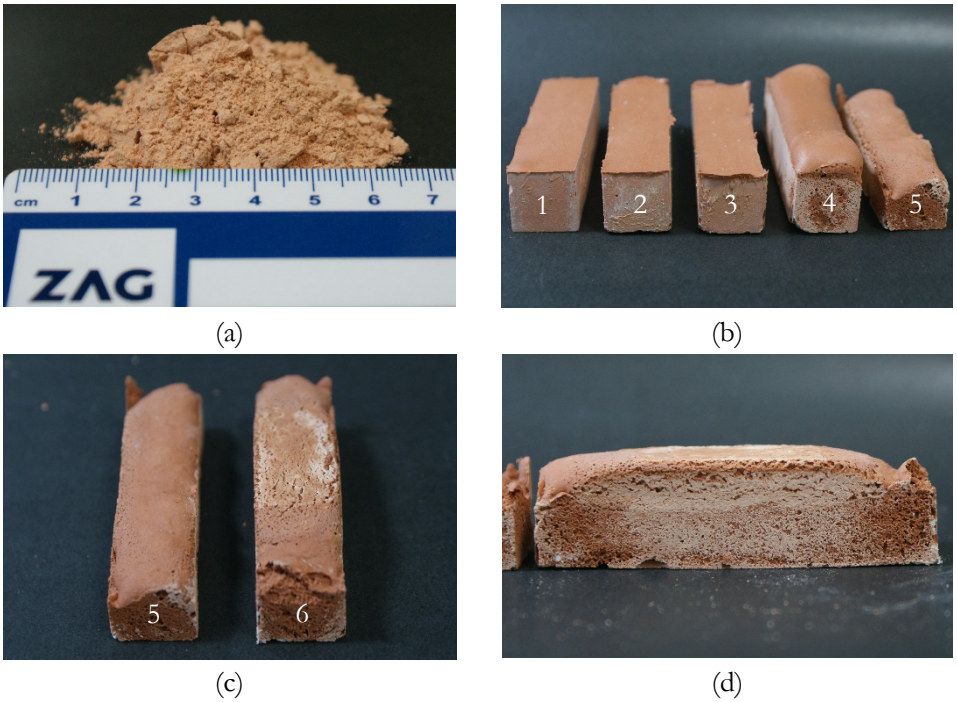

(a) (b)

(c) (d)

Figure 2: Photography of (a) MK and its (b) alkali-activated counterparts (cured at 1) room conditions, 2) and 3) at 100 W for 1 min in 2) open and 3) closed mould, 4) and 5) at 1000 W for 1 min in 4) open and 5) closed mould). (c) Alkali-activated MK cured for 1 min at 1000 W in the closed mould where prism 5) did not reach the cover, 6) and (d) reached the cover of the mould during "foaming".

Source: own.

H_2O in the initial slurry was mainly from Na-water glass and accounted for 20.9% of the combined mass of precursor and Na-water glass. The measured moisture of MK was 0.5%, indicating that the initial amount of water in the slurry (corrected for the moisture in the precursor) was approximately 21.0%.

Total mass losses were about 13.7% for the 1-year-old non-irradiated sample and 21.5% for the fresh, non-irradiated and not-hardened sample. About 21.1% for the sample irradiated at 100 W for 1 min and similarly for the covered sample, i.e., the total mass loss was about 21.3%. For non-irradiated and the 100 W irradiated samples, the total mass loss a slightly less than the total "theoretical" initial amount of water (which could be due to the human error in weighing the ingredients or/and to degradation of compounds present in "trace" amounts in the slurry and in AAM/AAF). Therefore, irradiation for 1 min at 100 W had no effect on dehydration and crack-pore formation.

The total mass loss of the sample irradiated at 1000 W for 1 min was about 11.4% and very similar results were obtained for the covered alternative, i.e., the mass loss was about 13.6%, as shown in Figure 3. This value is comparable to the mass loss of the non-irradiated aged sample, leading to the conclusion that the slurry irradiated with higher microwave power completed the long-term aging process in only 1 min. This was possible only in the case of extreme dehydration accompanied by pore-formation (Figure 2).

In both cases of covered/uncovered samples, i.e., irradiated at 100 W and 1000 W, the mass loss was higher for the covered samples, which is attributed to the retention of water in the covered sample during microwave irradiation and the successful hindering of dehydration. While synthesis in covered moulds can be described as hydrothermal synthesis at lower pressure (and with the possibility of release depressurizing by lifting the cover when the pressure reaches 235 Pa), cooking, synthesis in open moulds can be described as "baking".

The TG curves show that significant mass losses occur in two temperature ranges, (i) from room temperature to 200 °C due to the evaporation of free water adsorbed on the surface, as well as the retained water trapped in the pores of the sample, and some chemically bonded water, and (ii) between 200 °C and 600 °C, where mass losses range from 1.1% to 2.7%. In this temperature range, the mass loss is mainly due to evaporation of retained chemically bound water and dehydroxylation of unreacted kaolinite, which occurs between 400 °C and 600 °C (Alshaaer et al., 2016) and vary between 0.2 and 1%. Samples irradiated at 1000 W had lower mass losses in this range, indicating that irradiation already affected compounds decomposing in

the 200 °C to 600 °C range. Lower mass losses were again for samples irradiated at 1000 W, indicating that the irradiation most likely affected the crystal structure of the kaolinite and made it available for the alkali-activated reaction. Lower mass losses from about 700 °C could be due to CO_2 losses from calcite (Frost et al., 2009), which, interestingly, are significantly higher in both cases of irradiation at 1000 W, i.e., covered and not covered, as shown in Table 4. This means that the small amount of Ca present in MK contributes in ASN, onlly that it did not have enough time to dissolve in less than 1 min of high-power microwave irradiation.

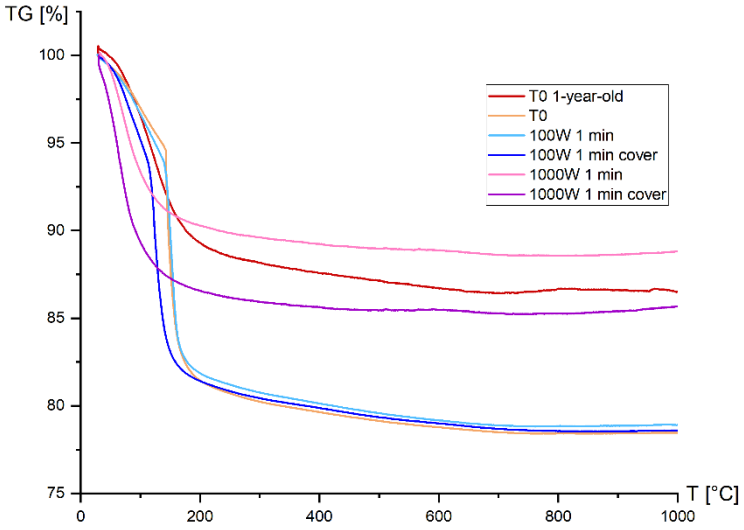

Figure 3: TG of alkali-activated samples: 1-year-old non-irradiated sample (red), fresh non-irradiated sample (orange), sample irradiated at 100 W for 1 min (light blue), its covered alternative (dark blue), sample irradiated at 1000 W for 1 min (light pink), and its covered alternative (dark pink).

Source: own.

Figure 4 shows the DTA curves. The fresh, non-irradiated sample and the sample irradiated at 100 W for 1 min (orange and light blue curves, respectively), which have the largest mass loss up to 200 °C, also have the narrowest and most pronounced course of the curve. They are followed by the sample irradiated at 100 W for 1 min while covered (dark blue curve) and then the sample irradiated at 1000 W for 1 min (dark pink curve), which was also covered during microwave irradiation. The 1-year-old non-irradiated sample (red curve) and the sample irradiated at 1000 W for 1 min

(light pink curve), which show the lowest mass loss in the temperature range up to 200 °C, have a broad curve shape and the least endothermic peak. The curve shape of a one-year-old sample differs from freshly prepared samples, which have a much larger and narrower endothermic curve. The differences are due to the fact that 1-year-old sample does not contain as much free adsorbed water and the peak is smaller due to the smaller amounts of adsorbed water. The boader endothermic course of the curve is due to the presence of interstitial and bound water, which is released at higher temperatures than the free adsorbed water. Also, the not-covered sample irradiated at 1000 W for 1 min shows a lower peak, which is due to dehydration during microwave irradiation. The adsorbed water content in this sample is also lower than in the others, as can be seen from the TG curves in Figure 3 and Table 4.

Table 4: Total mass loss and mass loss over different temperature ranges.

Samples	Total mass loss [%]	Mass loss over different temperature ranges			
		T0-200 °C [%]	200-600 °C [%]	400-600 °C [%]	> 700 °C [%]
T0 1-year-old	13.8	11.1	2.6	0.9	0.1
T0	21.4	18.4	2.7	0.9	0.04
100 W 1 min	20.9	18.0	2.7	1.0	0.03
100 W 1 min covered	21.3	18.5	2.4	0.9	0.1
1000 W 1 min	11.4	9.9	1.4	0.4	0.2
1000 W 1 min covered	13.6	12.7	1.1	0.2	0.4

All samples also show a small endothermic peak just before 600 °C, which is attributed to the endothermic dehydroxylation reaction, which, according to the literature, occurs somewhere between 530 and 590 °C (Deju et al., n.d.).

Moisture (Table 5) in the alkali-activated samples was highest in sample cured only at room conditions, while the other samples had less moisture, but not more than 4% less when 3 days old and not less than 1.5% when 8 days old. Comparing the TG mass loss in the range of room temperature to 200 °C for a 1-year-old sample (Table 4) and its moisture content (Table 5), there could be about 4.5% chemically bound water. Dehydration of the slurries at room temperature is most pronounced in the samples prepared without irradiation and samples irradiated with microwaves of 100 W. The difference between the TG mass loss in the range between T0 and 200 °C (Table 4) and the measurement of moisture after 3 days (Table 5) is between

5% and 6% for the mentioned samples, while for the samples irradiated at 1000 W this difference is less significant. However, dehydration continues and the amount of moisture in all samples after 28 days is comparable to or close to the final equilibrium for samples left at room conditions.

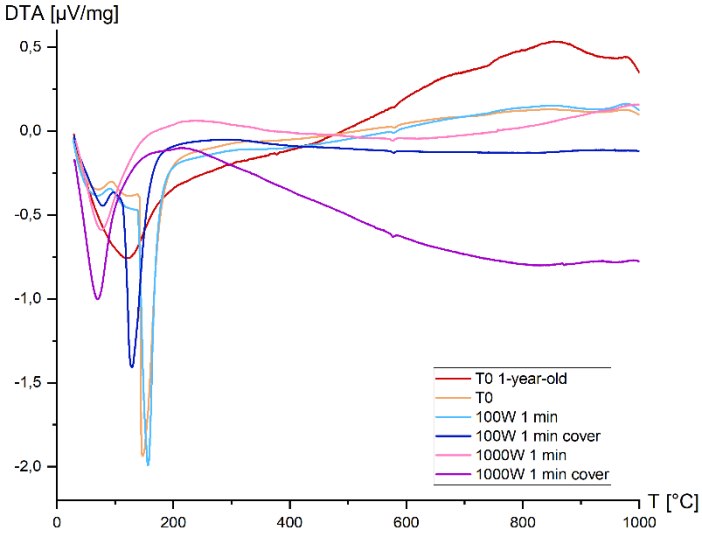

Figure 4: DTA of alkali-activated samples: 1-year-old non-irradiated sample (red), fresh non-irradiated sample (orange), sample irradiated at 100 W for 1 min (light blue), its covered alternative (dark blue), sample irradiated at 1000 W for 1 min (light pink), and its covered alternative (dark pink).

Source: own.

Table 5. Moisture in 3-day-old and 28-day-old alkali-activated samples was determined by IR heating at 105 °C.

Sample	T0	100 W 1 min	100 W 1 min covered	1000 W 1 min	1000 W 1 min covered
Moisture 3 days [%]	13.5	11.8	12.0	9.7	13.1
Moisture 28 days [%]	7.8	6.7	7.1	6.5	7.5
Moisture 1-year-old [%]	6.6	/	/	/	/

Compressive and bending strengths, the most important parameters for structure-functional products in building and civil engineering, are shown in Figure 5 and Table 6. For all three AAMs (sample prepared at room temperature, and both

samples irradiated at 100 W), geometric densities are identical, but the compressive strengths differ significantly. However, after 28 days, all samples reach comparable values of mechanical strengths, while thee geometric densities decrease uniformly for all of them. The conclusion is that low-power microwave irradiation enhanced the early reactions (dissolution, diffusion, self-assembly, i.e., networking-gelation of ASN) and curing without affecting dehydration. The final internal chemistry of ASN probably did not change, as did the porosity and amount of ASN.

For foamed samples, as expected, a large decrease in geometric densities of both AAFs (samples irradiated at 1000 W) resulted in a large decrease in early compressive strength. AAF prepared in closed mould exhibited lower compressive and bending strengths, most likely due to the of pore structure and ASN framework collapsing under the pressure of the limited space for material expansion during foaming (Figure 2, (c) and (d)). With time, the mechanical strengths increased, but the compressive strength reached only approximately 15% of the highest compressive strength of the 28-day-old AAM.

The relative error of the early measurement of mechanical strengths (standard deviation) increased with microwave power. This increase in comparison with AAM, which was prepared exclusively under room conditions, is a consequence of the non-uniform distribution of microwaves in the microwave. The reason for the huge increase in the relative error of the AAFs was mainly a consequence of the large decrease in mechanical strengths. With time, the absolute error of the compressive strength of the AAMs increased, which means that the samples need more time to reach the final values of mechanical strength.

The effect of microwave irradiation on the immobilization of trace and minor elements was tested by leaching experiments and the results are shown in Table 7. The concentrations of the elements are compared with the legislation values specified in the Decree on Waste Landfills. For the leaching experiments, the leaching of precursor (MK) and AAMs was performed. MK shows concentrations of all elements below the inert waste limit. However, for the AAMs, the activation process was found to increase the leaching potential for Cr, Ni, Cu, and As, while the concentrations of the other elements were comparable to those of the precursor. In addition, the concentrations of AAMs for Cr and As exceeded the limits for inert

(As in samples prepared at 100 W and Cr in samples prepared at 1000 W) and in some cases even for non-hazardous waste (As in samples prepared at 1000 W). This suggests that microwave irradiation accelerates the leaching of As and Cr when exposed to high working power. However, for As and Cr, we did not observe any difference when the samples were cured at room temperature or irradiated at 100 W.

Table 6: Compressive and bending strength, their absolute and relative error, and geometric density of 3-days-old and 28-days-old alkali-activated samples.

3-days-old samples	CS [MPa]	σ_{CS} [MPa]	σ_{CS} [%]	BS [MPa]	σ_{BS} [MPa]	σ_{BS} [%]	ϱ [kg/dm^3]
T0	34.9	5.0	14.2	7.6	0.3	4.2	1.9
100 W 1 min	51.6	8.5	16.5	7.8	0.7	8.5	1.9
100 W 1 min cover	64.8	2.5	3.9	8.2	0.8	10.0	1.9
1000 W 1 min	9.1	2.5	27.5	4.0	0.9	23.7	1.2
1000 W 1 min cover	2.1	0.8	32.4	2.0	0.3	17.2	1.0
28-days-old samples	CS [MPa]	σ_{CS} [MPa]	σ_{CS} [%]	BS [MPa]	σ_{BS} [MPa]	σ_{BS} [%]	ϱ [kg/dm^3]
T0	66.0	13.4	20.4	9.1	0.6	7.1	1.7
100 W 1 min	67.8	12.0	17.7	10.5	0.8	7.3	1.7
100 W 1 min cover	66.8	11.6	17.4	10.1	0.1	1.1	1.8
1000 W 1 min	11.9	7.1	59.6	6.6	2.6	38.6	1.2
1000 W 1 min cover	9.2	1.7	18.3	3.6	0.4	10.3	1.0

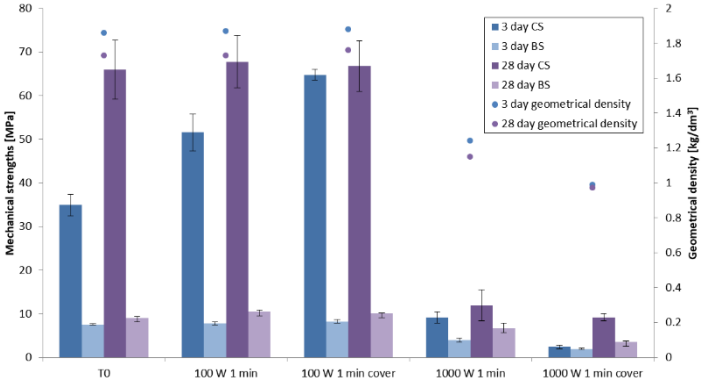

Figure 5: Compressive (CS) and bending (BS) strengths with geometric densities of 3-days-old and 28-days-old alkali-activated samples.

Source: own.

Table 7: The concentrations in mg/kg of selected elements were measured in the digested samples and leachates according to SIST EN:12457-2 standard protocol.

Element [mg/kg]	Cr	Ni	Cu	Zn	As	Se	Mo	Cd	Sb	Ba	Hg	Pb
MK	0.22	0.0004	0.0008	0.004	0.08	0.06	0.02	<0.002	0.002	0.02	<0.001	0.0001
AAM T0	0.20	0.03	0.03	0.010	0.62	0.03	0.03	<0.002	0.003	0.003	0.003	0.005
AAM 100 W 1 min	0.17	0.02	0.03	0.007	0.57	0.03	0.02	<0.002	0.002	0.004	0.002	0.005
AAM 1000 W 1 min	0.97	0.02	0.02	0.005	2.66	0.08	0.07	<0.002	0.006	0.003	0.002	0.002
Inert waste*	0.5	0.4	2.0	4.0	0.5	0.1	0.5	0.04	0.06	20.0	0.01	0.5
Non-hazardous waste*	10.0	10.0	50.0	50.0	2.0	0.5	10.0	3	0.7	100.0	0.20	10.0

*Decree on waste landfill: http://www.pisrs.si/Pis.web/pregledPredpisa?id=URED6660#

4 Conclusion

When microwave irradiation of sufficiently high power was used in the very early stages of alkali-activated slurry curing, the alkali-activation process ended in a very short time as alkali-activated foam. At lower microwave powers, the alkali-activated samples ended up as non-foamed alkali-activated materials with much higher early mechanical strengths compared to the non-irradiated reference, but the curing time was not shortened, i.e., the microwaves only enhanced early-stage dissolution in alkali-activated synthesis.

From the thermogravimetric analysis, it is evident that the power of microwave irradiation has a significant effect on the course of the curves. Differences are also observed between uncovered samples during microwave irradiation and covered samples during microwave irradiation, which complicates the evaporation of water during irradiation. The 1-year-old sample was found to be most similar to the sample irradiated at 1000 W for 1 min. TG/DTA analysis showed that microwave irradiation at lower microwave powers (100 W) for 1 min did not result in significant differences compared to the non-irradiated samples.

Alkali-activation did show an increase in leaching of As, low powers of irradiation with microwaves did not have additional influence on it, while high irradiation powers additionally increased leaching of As and Cr.

Concentrations for most of the toxic trace and minor elements were low except for As and Cr. Cr exceeded the limit for inert waste when alkali-activated slurries were irradiated at 1000 W, whereas As exceeded values for inert waste for all AAMs. Moreover, in the case of samples irradiated at 1000 W, Cr exceeded the values also for non-hazardous waste. Research showed that irradiation at higher working power decreased the immobilization potential of As, i.e. microwaves shows potential to remove heavy elements from dangerous materials and thus could present efficient method for recovery or remediation.

Acknowledgement

This work is part of the ARRS project of dr. Barbara Horvat and was financially supported by the Slovenian Research Agency under Grant no. J2-3035.

This work is part of the postdoc project of dr. Majda Pavlin and was financially supported by the Slovenian Research Agency under Grant no. Z2-3199.

References

Alshaaer, M., El-Eswed, B., Yousef, R.I., Khalili, F., Rahier, H., 2016. Development of functional geopolymers for water purification, and construction purposes. Journal of Saudi Chemical Society 20, S85–S92. https://doi.org/10.1016/j.jscs.2012.09.012

Ameri, F., Shoaei, P., Zareei, S.A., Behforouz, B., 2019. Geopolymers vs. alkali-activated materials (AAMs): A comparative study on durability, microstructure, and resistance to elevated temperatures of lightweight mortars. Construction and Building Materials 222, 49–63. https://doi.org/10.1016/j.conbuildmat.2019.06.079

Burkhard Walther, Bernhard Feichtenschlager, Shengzhong Zhou, 2017. Self-foaming Geopolymer Composition COntaining Aluminum Dross. US 9,580,356 B2.

Deju, R., Cucos, A., Mincu, M., Tuca, C., n.d. Thermal characterization of kaolinitic clay 8.

Duxson, P., Provis, J.L., Lukey, G.C., Mallicoat, S.W., Kriven, W.M., van Deventer, J.S.J., 2005. Understanding the relationship between geopolymer composition, microstructure and mechanical properties. Colloids and Surfaces A: Physicochemical and Engineering Aspects 269, 47–58. https://doi.org/10.1016/j.colsurfa.2005.06.060

Fletcher, R.A., MacKenzie, K.J.D., Nicholson, C.L., Shimada, S., 2005. The composition range of aluminosilicate geopolymers. Journal of the European Ceramic Society 25, 1471–1477. https://doi.org/10.1016/j.jeurceramsoc.2004.06.001

Frost, R.L., Hales, M.C., Martens, W.N., 2009. Thermogravimetric analysis of selected group (II) carbonateminerals — Implication for the geosequestration of greenhouse gases. J Therm Anal Calorim 95, 999–1005. https://doi.org/10.1007/s10973-008-9196-7

Hajimohammadi, A., Ngo, T., Mendis, P., Kashani, A., van Deventer, J.S.J., 2017a. Alkali activated slag foams: The effect of the alkali reaction on foam characteristics. Journal of Cleaner Production 147, 330–339. https://doi.org/10.1016/j.jclepro.2017.01.134

Hajimohammadi, A., Ngo, T., Mendis, P., Sanjayan, J., 2017b. Regulating the chemical foaming reaction to control the porosity of geopolymer foams. Materials & Design 120, 255–265. https://doi.org/10.1016/j.matdes.2017.02.026

Horvat, B., Ducman, V., 2020a. Influence of curing/drying methods including microwave heating on alkali activation of waste casting cores, in: COMS 2020. Presented at the 2nd International Conference on Construction Materials for Sustainable Future, Bled, Slovenia.

Horvat, B., Ducman, V., 2020b. Influence of Particle Size on Compressive Strength of Alkali Activated Refractory Materials. Materials 13, 2227. https://doi.org/10.3390/ma13102227

Horvat, B., Ducman, V., 2019. Potential of Green Ceramics Waste for Alkali Activated Foams 30.

Marvila, M.T., Azevedo, A.R.G. de, Vieira, C.M.F., 2021. Reaction mechanisms of alkali-activated materials. Rev. IBRACON Estrut. Mater. 14, e14309. https://doi.org/10.1590/s1983-41952021000300009

Pacheco-Torgal, F., Castro-Gomes, J., Jalali, S., 2008. Alkali-activated binders: A review. Part 2. About materials and binders manufacture. Construction and Building Materials 22, 1315–1322. https://doi.org/10.1016/j.conbuildmat.2007.03.019

Provis, J., 2013. Alkali activated materials: state-of-the-art report, RILEM TC 224-AAM. Springer, New York.

Rincón Romero, A., Toniolo, N., Boccaccini, A., Bernardo, E., 2019. Glass-Ceramic Foams from 'Weak Alkali Activation' and Gel-Casting of Waste Glass/Fly Ash Mixtures. Materials 12, 588. https://doi.org/10.3390/ma12040588

Škvára, F., 2007. Alkali Activated Material - Geopolymer 16.

Tokoro, C., Suzuki, S., Haraguchi, D., Izawa, S., 2014. Silicate Removal in Aluminum Hydroxide Co-Precipitation Process. Materials 7, 1084–1096. https://doi.org/10.3390/ma7021084

Wei, Y.-L., Cheng, S.-H., Ko, G.-W., 2016. Effect of waste glass addition on lightweight aggregates prepared from F-class coal fly ash. Construction and Building Materials 112, 773–782. https://doi.org/10.1016/j.conbuildmat.2016.02.147

PILOT PRODUCTION OF FAÇADE PANELS: VARIABILITY OF MIX DESIGN

MAJDA PAVLIN, BARBARA HORVAT, VILMA DUCMAN
Slovenian National Building and Civil Engineering Institute, Ljubljana, Slovenia
majda.pavlin@zag.si, barbara.horvat@zag.si, vilma.ducman@zag.si

Abstract As part of the WOOL2LOOP project, the Slovenian National Building and Civil Engineering Institute (ZAG), in collaboration with Termit d.d. were responsible for the production of façade panels. An initial mix design was developed at ZAG, where alkali-activated façade panels were produced, primarily from stone wool waste, while production took place at Termit. The mix design was changed twice during the pilot production, before a final product with suitable durability was developed. A compressive strength of up to 60 MPa and bending strength of approximately 20 MPa was achieved. The mechanical properties, however, varied, due to the unevenly milled batches of the milled mineral wool. Milling on a larger scale is very challenging, and it is difficult to obtain consistent quality of the milled material. Once the correct curing process had been found, however, the panels produced showed good performance. Moreover, the results from leaching tests showed that the elevated concentrations of certain elements (Cr, As and Mo) did not exceed the legal limits for non-hazardous waste.

Keywords:
waste mineral wool,
façade panels,
alkali-activated material,
recycling,
leaching,
mechanical properties

University of Maribor Press
DOI https://doi.org/10.18690/um.fkkt.1.2023.3
ISBN 978-961-286-692-1

1 Introduction

Mineral wool is one of the most widely used insulation materials in the world. As a result, its disposal poses a major problem at the end of its use, taking up a lot of space in landfills due to its low density. In 2020, the European Union generated approximately 2.55 million tons of mineral wool waste, which represents only about 0.2% of the total amount of construction and demolition waste produced in the European Union. Most construction and demolition waste is recyclable, while mineral wool is considered to be non-recyclable (Väntsi and Kärki, 2014). There is therefore an urgent need to find a way to recycle, reuse or recover these wastes. Mineral wool is usually divided into two categories - stone and glass wool - which differ in terms of both their chemical composition and the raw materials used in their production (Müller et al., 2009; Kowatsch, 2010). Stone wool accounts for about 70% of the mineral wool produced worldwide (Väntsi and Kärki, 2014). Under the Wool2Loop project the consortium has developed and produced various products with alkali activation technology, using mineral wool as the main raw material (precursor). Alkali activation is based on a chemical reaction that can produce end products that have similar or better properties than concrete or ceramic-type products. Some studies have already been conducted where mineral wool was alkali-activated, either alone or in combination with other co-binders (Yliniemi et al., 2016; Kinnunen et al., 2017). Although, theoretically, mineral wool waste is an ideal starting material, because almost 100% of this waste is in the amorphous phase, in reality not all fibres dissolve during alkali activation (Pavlin et al., 2021a). This should be taken into account, because problems with efflorescence can occur if too much of the alkali activator is added.

In the present work, architectural façade panels were developed. The selected mix design (Pavlin et al., 2022) consisted of mineral wool waste as the main raw material, with local slag (a mixture of electric arc furnace slag and ladle slag), metakaolin and lime added as co-binders. Mix design developed and selected in the lab was modified two times. The prepared façade panels was monitored by measuring the mechanical properties of the alkali-activated material (AAM), the particle size distribution in randomly selected samples, mineralogy, open porosity, the degree of alkali activation and leaching parameters used to evaluate the environmental impact.

2 Material and methods

Sample preparation: Stone wool (SW) was used as the primary precursor for the preparation of façade panels. Milled material was obtained from the company ISOMAT (Slovenia). A sodium silicate obtained from Termit d.d. (sodium silicate activators with a molar ratio-module of approximately SiO_2/Na_2O = 2.5; and mass percent 11.9% Na_2O, 28.5% SiO_2) was used for the alkali activation. Various co-binders, including local slag (S; commercially available electric arc furnace slag mixed with ladle slag and branded as secondary by-product EKOMINIT; milled and sieved below 125 μm), metakaolin (MK; used as received) and lime (L; used as received) were also added to the mineral wool precursor. As aggregate (AG) quartz sand (MP-MIX) from Termit d.d. was used for all prepared mix designs. After mixing all the dry precursors together, sodium silicate was added and mixed until the slurry was completely wet, and then the slurry was poured into moulds made of silicone or urethane rubber. For optimisation of mix design, at first, the samples were cured at room temperature in closed PVC bags to hinder dehydration. Then after three days, the façade panels were exposed to an elevated temperature (60 °C at 30, 60 or 90% humidity; humidity chamber POL-EKO APARATURA, Poland).

Analysis of the precursors and AAMs: Chemical (X-ray fluorescence, XRF; Thermo Scientific ARL Perform'X Sequential XRF) and mineralogical (X-ray powder diffraction, XRD; Empyrean PANalytical X-ray Diffractometer, Cu X-Ray source) analyses of SW, S, M and L were conducted. All the precursors were dried, milled and sieved to below 125 μm prior analyses. XRF measurements were performed on molten discs and analysed using UniQuant 5 software. The data measured are provided in Table 1.

Table 1: Chemical composition of the precursors (stone wool, lime, metakaolin and local slag) used for the alkali activated façade panels.

Chemical composition of precursors	SiO_2 (wt%)	Al_2O_3 (wt%)	Na_2O (wt%)	CaO (wt%)	MgO (wt%)	Fe_2O_3 (wt%)	LOI (950 °C)
Stone wool (SW)	38.4	17.2	2.00	16.1	11.6	6.45	4.60
Lime (L)	1.86	2.05	0.30	68.2	2.07	0.10	24.8
Metakaolin (M)	68.1	25.2	0.09	0.45	0.16	2.21	2.25
Local slag (S)	13.7	5.20	0.28	27.9	23.3	4.64	20.5

The XRD patterns were solved using X'Pert Highscore plus 4.1 software. Rietveld refinement was performed with an external standard (corundum, Al_2O_3) to estimate the content of amorphous content and minerals. XRD spectra of the precursors used in the alkali activation process are provided in **Figure 1**.

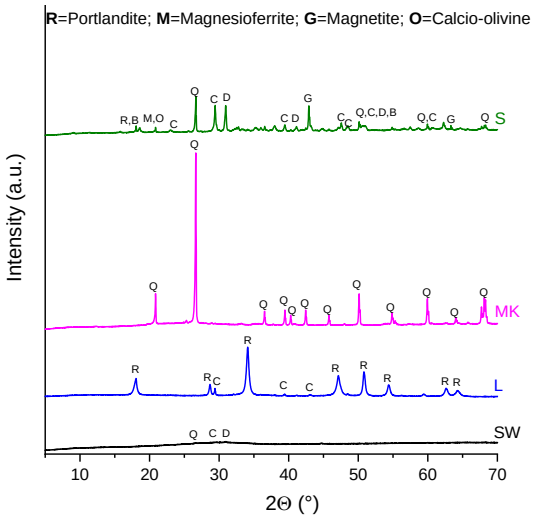

Figure 1: Diffractograms of the precursors (SW, L, MK and S) used for preparation of the façade panels.

Source: own.

Open porosity of alkali-activated façade panels was determined using mercury intrusion porosimetry (MIP). Small representative fragments about 1 cm^3 in size were dried for 24 h before measurement and then analysed using Micromeritics®Autopore IV 9500 equipment (Micromeritics, Norcross, GA, USA).

28 days after placing samples in the moulds the mechanical strength (bending and compressive) of the AAMs was measured using a compressive and bending strength testing machine (ToniTechnik ToniNORM).

The presence of toxic elements in leachates was evaluated after 28 days according to the European standard SIST EN 12457-2. The AAM was crushed to a grain size of below 4 mm and added to a glass bottle containing deionised water using a solid:liquid mass ratio of 1:10. The suspensions were rotated around the vertical axis for 24 h at room temperature conditions, and then filtered to below 0.45 μm. An

aliquot of the coloured liquid fraction obtained (Figure 2, the typical yellow-brown colour is a consequence of organic resin or other organic compounds present on the surface of the milled waste mineral wool) was digested in the microwave, then the clear solutions prepared were used to determine the amount of metals released using an inductively coupled plasma mass spectrometer (ICP-MS, Agilent 7900). The results were compared to the total amount of toxic trace and minor elements measured in the precursor, as well as to figures from the legislation (Decree on Waste Landfill (Official Gazette of Republic Slovenia, 2014)).

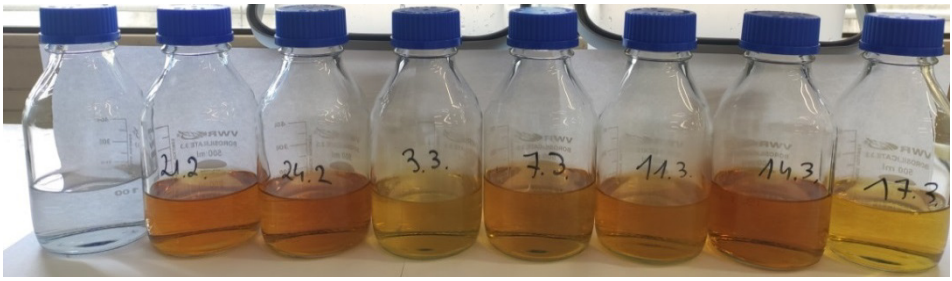

Figure 2: Leachates from the alkali activated façade panels obtained following filtration to below 0.45 µm. The transparent liquid in the bottle on the left is a blank, without the addition of a sample.
Source: own.

3 Results

3.1 The results of milling process

The mineral wool was pre-milled by a Slovenian company, and the mass ratio of the finest particle size (< 63 µm) over the time of the study is shown in Figure 3. When the development of initial mix design (described in details in 3.2.) had started (i.e. mix design 1), the finest fraction of mineral wool waste accounted for more than 60 wt% of total content (Figure 3; milled mineral wool samples 1-4). When upscaling mix design 1, the slurry was too liquid, and the amount of sodium silicate and waste mineral wool was adjusted, and this lead to development of mix design 2. After changing the grinding parameters in the company that performed this, the quality of the milled mineral wool decreased (Figure 3; milled mineral wool sample 5) and production of the façade panels was faced with various problems, starting with poor

workability of mix desing 2. Besides problems with initial fresh mixture, the already cured panels exhibited curvature, high structural porosity and the occurrence of the efflorescence. The situation became even worse with the milled mineral wool samples 6-8 (Figure 3), where the proportion of the finest fraction represented only a few mass percent of the total content. From that point forward, additional milling was implemented by Termit using a concrete mixer (i.e. ball milling). With double-milled mineral wool it was possible to prepare mix design 1 again, but to minimize the efflorescence, mix design 3 was developed. This mixture was then used in the pilot production.

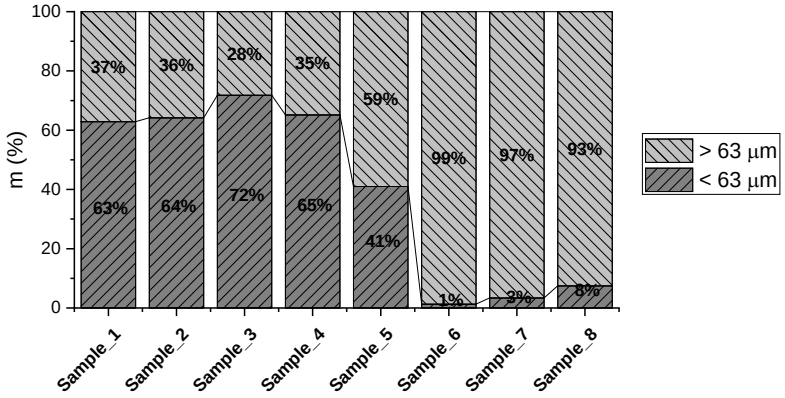

Figure 3: The particle size distribution of the finest fraction (< 63 μm) versus other fractions (> 63 μm) in the (pre)milled mineral wool.

Source: own.

3.2 Preparation of façade panels: optimisation of selected mix design

The façade panels prepared from mineral wool and other co-binders need to have suitable mechanical properties, and be both durable and environmentally-friendly (in terms of their parameters regarding leaching toxic metals and other toxic substances). Following use of the initial mix design (mix design 1) in the pilot production, some modifications were then made to the mix design at the beginning of pilot production (mix design 2; the mixture was too liquid so less sodium silicate was used and the proportion of mineral wool was increased, as shown in Table 2). After that, based on many problems with the façade panels with respect to curvature,

porosity, efflorescence, workability and demoulding time, the mix design had to be modified again during the pilot production. The last change in the mix design (to developed mix design 3) was made mainly due to the observed curvature and difficult mixing of the very viscose slurry while aiming for perfect wetting of the pulverized precursor's particles (poor workability of the mixes as a result of the unevenly ground mineral wool batches, Figure 3). The original mix design developed in the lab and used for pilot production (mix design 1), the modified mix design (mix design 2), and the final mix design (mix design 3), are defined in Table 2. Mix designs 1 and 2 were cured at room temperature, while mix design 3 was cured for three days at room temperature covered with PVC to hinder the dehydration and allow slow-reacting precursor enough time for initial curing before demoulding (Pavlin et al., 2021a), and then at 60 °C and 60% humidity on level metal mesh for uniform drying of all 6 panel's sides. There are some differences between the various mixes; due to the presence of efflorescence, for example, NaOH was removed from the mix design 3 and the amount of sodium silicate reduced (in mix design 2 and 3), also the amount of used waste mineral wool differ (Table 2).

The compressive and bending strengths of the initial mix developed in the laboratory (mix design 1) cured at room temperature for 28 days were (42.5 ± 2.7) MPa and (14.3 ± 2.1) MPa, respectively, while the compressive and bending strengths of mix design 2 (also cured at room temperature) were lower (33.3 ± 3.1) MPa and (11.3 ± 0.5) MPa, respectively. Mix design 3, cured three days at room temperature and three days at 60 °C and 60% humidity, showed similar mechanical properties to mix design 1 after 28 days of curing at room temperature, with a compressive strength of (41.0 ± 7.1) MPa and a bending strength of (15.3 ± 0.4) MPa.

The workability of mixtures is very important, especially at the industrial level of pilot production. It was evaluated using a slump test by measuring the spread of the mortar. The data for prepared mixtures can be found in Table 2 (slump test; the good workability of prepared mortars is usually in the range of 165-185 mm (Pavlin et al., 2022)). Workability depends on the particle size of the starting materials as a result of the grinding process. In the case of mineral wool, a higher amount of the fraction > 63 μm - larger particles, require more liquid (sodium silicate) to achieve the desired workability of the mixture, and therefore mixing was difficult with the same amount of sodium silicate and larger particles, and vice versa, smaller particles

require less liquid. Moreover, the dense mixture did not result in any changes in the spreading of the slurry in the slump test (the diameter measured on the spreading table remained the same). Mix design 1 contained the highest amount of sodium silicate and showed the highest spread whereas mix design 2 and 3 had the same spread (the results of slump test in Table 2).

Table 2: The original mix design (mix design 1), developed in the lab of ZAG, the modified mix design (mix design 2) and mix design currently in use (mix design 3).

Mix design	SW (g)	Sodium silicate (g)	NaOH (g)	L (g)	M (g)	S (g)	AG (g)	Slump test (mm/mm)
1 (original)	29.9	42.7	0.47	0.85	7.67	4.26	14.2	172/183
2	33.9	39.8	0.46	0.97	7.47	3.59	13.8	165/170
3 (current mix)	33.1	37.6	/	0.95	8.51	4.72	15.1	165/170

At the beginning of the pilot production, panels were demoulded after one day (mix design 1) (Pavlin et al., 2022). Using batches of milled mineral wool with a higher mass percentage of big particles (> 63 μm, Figure 3) this was no longer possible due to the change in the particle size after milling. Therefore, the curing conditions were optimized; first, curing was performed at room temperature, then different conditions were tested (60 °C and humidity of 30, 60 or 90% (Pavlin et al., 2021b)). We also performed experiments at 40 °C, but the mechanical properties were lower and the curing times should be longer, therefore those results were excluded (Pavlin et al., 2021b). The results of the mechanical properties after testing different humidity at 60 °C can be found in Figure 4.

Panels cured at 60 °C and 30% humidity were not suitable and showed little curvature. A humidity of 90% was too aggressive for the curing oven, which was evident from the damaged support mesh caused by the high alkaline vapour resulting from the alkali activation process. 60 °C and 60 % humidity were selected as the most suitable curing conditions at which the façade panels did not exhibit the curvature. At the same time, tests were carried out with different amounts of lime, with the mixtures containing 1, 2, or 3 wt% lime. However, with 1 wt% lime, the specimens could not be demoulded after three days of curing at room temperature and exhibited curvatures, while with 3 wt% lime, mixing the mixtures was difficult due to the too fast hardening. Mix designs 1 and 2 with 2 wt% of lime showed no

curvature, but mix design 2 was difficult to prepare due to the viscous slurry. Therefore, mix design 1 with 2 wt% of lime was taken for further optimisation.

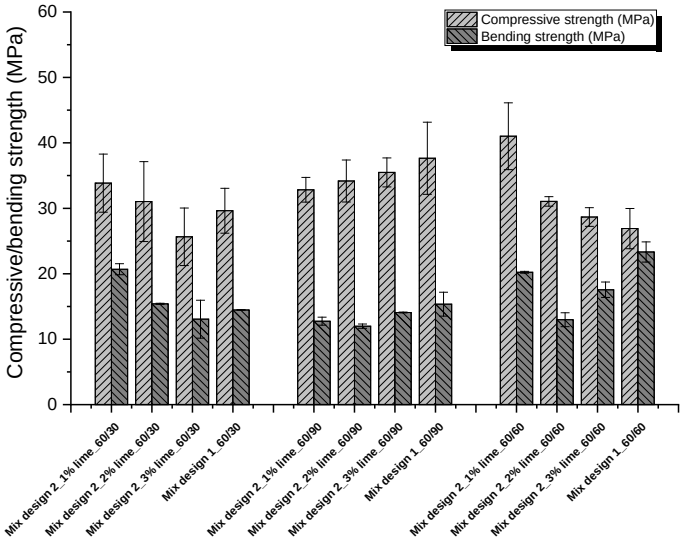

Figure 4: Samples cured three days at room temperature in closed bags and then three days at 60 °C with different humidity (30, 60 or 90%). 1, 2 or 3 wt% of lime were added in the mix design 2. Sample mix design 1 had 2 wt% of added lime.

Source: own.

After selecting the curing conditions (60 °C and 60% humidity), tests regarding the time of the additional milling and the variations in the amount of sodium silicate and NaOH were performed, which are shown in Figure 5. Mineral wool from sample batches 6-8 was used for this experiment (Figure 3). The workability of the mixtures, evaluated by the slump test, is presented in Table 3. Initially, mix design 1 was selected and mineral wool sieved below 125 μm was used. The workability of this mixture was suitable for further use, but unfortunately, the panel showed curvature. Then tests were carried out with different milling times (2, 4, 6 and 8 hours of additional grinding in the concrete mixer). The use of the wool after 2 and 4 hours of additional grinding was not suitable (the mixture was too dense). After 6 hours, the workability was better, but the mixture was still too viscose to be useful in the pilot production. On the other hand, after 8 hours of grinding, the mixture was too liquid, therefore the amount of sodium silicate was reduced. The sample "Mix design

1_milled 8h_lessSS2x" showed good workability and no curvature. However, to decrease the efflorescence, NaOH was removed from the mix design and therefore "Mix design 1_milled 8h_ lessSS2x _no NaOH" was selected as a mixture for further production of panels labelled as "mix design 3". "Mix design 2_no NaOH" showed good workability, but was not selected, because its slurry showed adhesiveness to the flow table (used for the slump tests) and was therefore not useful for industrial production (mixture design 2 was added for comparison purposes only; the results of slump tests in Tables 2 and 3 differ due to the additional grinding process shown in Table 3 in the case of mix design 2).

Table 3: Spread of the prepared panels.

Sample	Slump test (mm/mm)
Mix design 1_sieved<125 um	168/165
Mix design 1_milled 2h	Too viscose
Mix design 1_milled 4h	125/128
Mix design 1_milled 6h	162/168
Mix design 1_milled 8h	Too liquid
Mix design 1_milled 8h_lessSS	201/203
Mix design 1_milled 8h_lessSS2x	173/175
Mix design 1_milled 8h_lessSS2x_no	**165/170**
Mix design 2	182/192
Mix design 2_no NaOH	173/178

However, the mechanical properties of the prepared samples (Figure 5) did not differ that much, considering that some of the mixtures were too viscose and some too fluid.

The lowest compressive strength (about 30 MPa) was exhibited by the sample with mineral wool additionally ground for 2 hours (due to the poorer dissolution of amorphous Si and Al owing to the lack of liquid - sodium silicate). As mentioned earlier in the text, bigger particles needed more liquid and therefore mixing is difficult. Mix design 2 exhibited the lowest bending strength. The selected sample "Mix design 1_milled 8h_ lessSS2x_no NaOH" has not the highest compressive strength, but it was above 40 MPa while a bending strength of about 15 MPa was achieved.

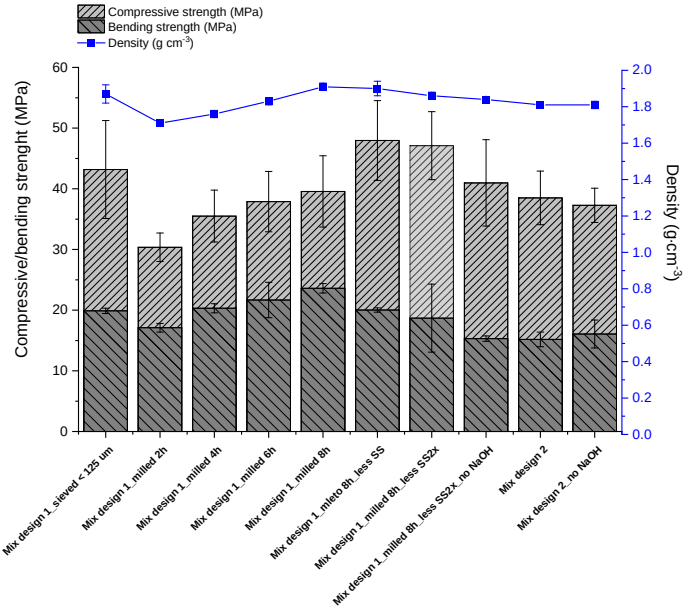

Figure 5: Different experiments were performed to find the optimal mix design. All samples were cured three days in closed bags and then three days at 60 °C and 60% of humidity.
Source: own.

3.3 Mix design 3: Variations in mechanical properties and correlations with particle size

Although the optimised mix design (mix design 3; Table 5) resulted in a mix with good workability, there were significant differences in mechanical properties between the different batches, as shown in Figure 6. The average compressive and bending strengths of 30 different prepared panels (made from several different batches) were 38.5 MPa ± 8.5 MPa and 14.9 MPa ± 3.2 MPa, respectively. Significant differences were also found in the density of the different specimens (1.64-1.91 g·cm^{-3}). Façade panels are required to have a compressive strength of at least 30 MPa (green line in Figure 6) and a bending strength of 10 MPa (grey line in Figure 6). It follows that most of the prepared panels met these requirements (Figure 6). The mechanical property results for 10 randomly selected batches are shown in Figure 7, along with particle size distribution analyses. However, the large differences between the different sample batches are due to the not consistent grinding of the mineral wool used to produce the panels (Figure 7). Although additional grinding in

Termit was performed, the large differences in particle size distribution between the batches affect the workability of the mixture and thus change the mechanical properties between the batches. A significant increase in compressive strength was observed when the smallest fraction (< 63 μm) was present in amounts of around 50 wt% (or more). Moreover, the workability of the mixture was better and the compressive strength higher (reaching up to 64 MPa) when the proportion of the smallest fraction in the mixture was higher (< 63 μm), as can be seen in **Figure 7**. The bending strength, on the other hand, is not necessarily related to the particle size distribution, since larger fibres could actually help improve the bending strength. Even with a smaller amount of the finer fraction (and thus an increased number of particles larger than 250 μm), the mechanical properties met the desired values previously determined.

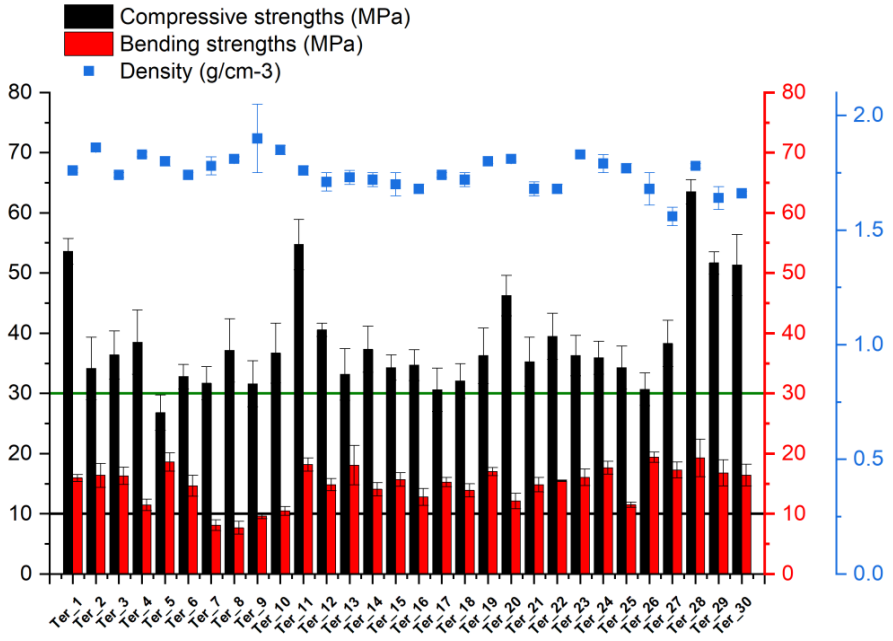

Figure 6: Compressive strength, bending strength and density of 30 different façade panels produced using the mix design 3. The values required are 30 MPa for compressive strength (green line) and 10 MPa for bending strength (grey line).

Source: own.

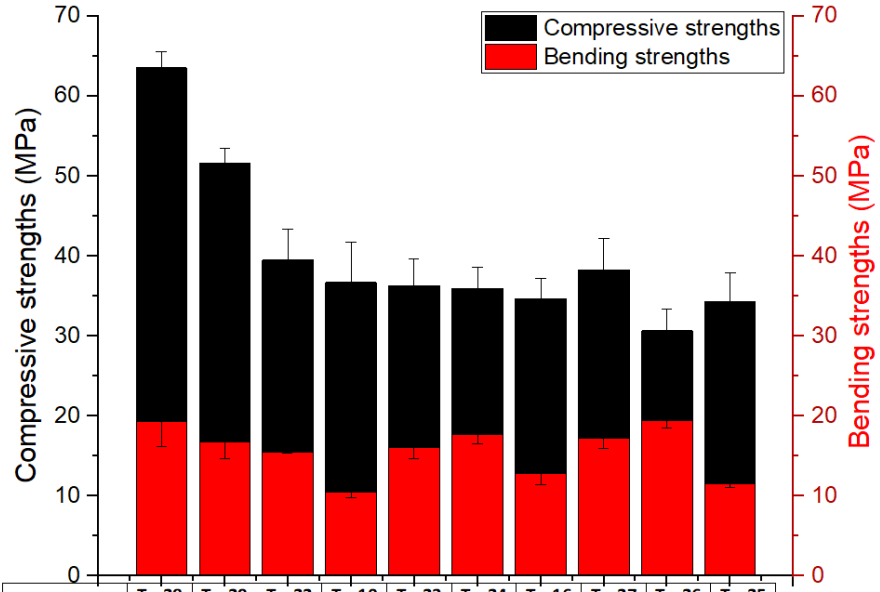

	Ter28	Ter29	Ter22	Ter10	Ter23	Ter24	Ter16	Ter27	Ter26	Ter25
< 250 µm (%)	96.3	98.6	92.6	100	93.5	87.0	93.5	88.1	67.4	54.0
< 125 µm (%)	79.9	86.5	79.5	42.9	72.3	69.9	75.3	61.4	46.0	38.7
< 63 µm (%)	55.1	45.7	39.9	26.6	24.1	20.3	19.1	15.2	10.1	9.41

Figure 7: The graph shows the compressive and bending strengths of 10 randomly selected mixtures where the particle size distribution was measured. The particle size distribution for particles sized < 63, < 125 and < 250 µm are provided in the table below the graph. The samples are arranged in descending order of proportion under 63 µm.

Source: own.

3.4 The results of selected mixtures: FTIR, open porosity, XRD and leaching of toxic trace and minor elements

In the next step, 12 different batches were selected from mixtures that exhibited different mechanical properties (30 different batches presented in Figure 6), and FTIR, open porosities, XRD and leaching analyses were performed.

The results of the FTIR analysis are provided in Figure 8. A transmission band at around 1644 cm^{-1} indicates the presence of an H–O–H bending vibration, due to the presence of water in the AAM. The humidity of these samples ranged between 4.0-5.6 wt% (measured after 28 days). In all samples, bands were seen at approximately 1450 cm^{-1} corresponding to the asymmetric stretching of CO_3^{2-} (O–

C–O), and a weak shoulder at around ~880 cm^{-1} due to the out-of-plane bending of CO_3^{2-}. This could be due to the presence of carbonate in the local slag precursor used in the mixture, and/or as a consequence of the carbonation process presented during the production of the façade panels (Yu et al., 1999). The main Si-O-T band (T = Si, Al) is between 990 and 1000 cm^{-1}. The shifts of the main Si-O-T bands, compressive strengths and open porosity of the samples are shown in Table 4. There is no correlation between the compressive strength and the band shift as well as with porosity values, suggesting that the alkali activation process (degree of polymerization) is similar for all samples and that the differences in mechanical properties are due to the different particle sizes distributions of the ground material.

Table 4: Compressive strengths, the position of the Si-O-T (T = Si, Al) asymmetric stretching vibration band and the data for open porosity.

Sample	Ter 11	Ter 12	Ter 13	Ter 14	Ter 15	Ter 16	Ter 17	Ter 18	Ter 19	Ter 20	Ter 21	Ter 22
Compressive strength	54.8	40.6	33.2	37.3	34.3	34.7	30.6	32.1	36.3	46.3	35.3	39.5
Si-O-T (T = Si, Al) (nm)	1000	999	991	1000	994	999	996	999	998	995	995	990
Open porosity (%)	18.8	24.4	22.1	24.9	21.5	17.9	24.0	15.6	21.4	20.5	26.5	27.8

C-A-S-H and/or C-S-H gels may form due to the presence of lime and local slag, whereas N-A-S-H is typically formed in the alkali-activated metakaolin. In stone wool activated with sodium silicate, however, (N,C)-A-S-H gel is suggested to be the prevailing form (Yliniemi et al., 2020). Since the mixture is composed of several precursors, the position of the bands, which were seen across all the samples, regardless of the batch, could belong to a mixture of gels (C-A-S-H, N-A-S-H (Garcia-Lodeiro et al., 2011) and (N,C)-A-S-H). Since quartz was used as an additional aggregate in the mixture, a doublet is seen at 797 and 778 cm^{-1}, as well as an additional band at 694 cm^{-1}.

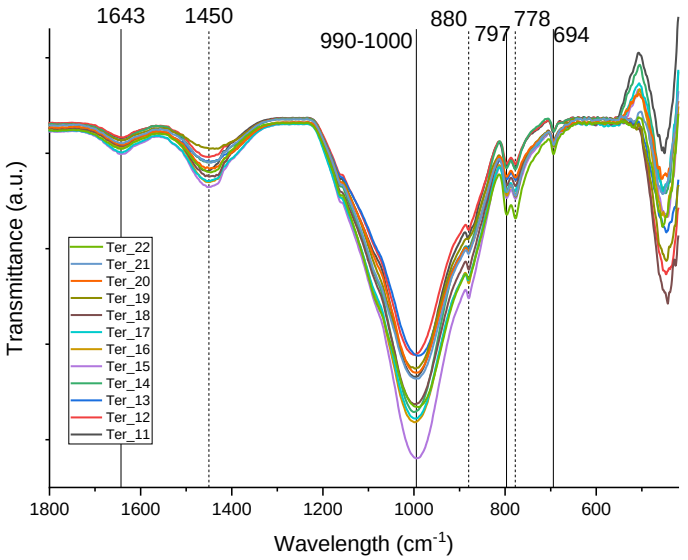

Figure 8: FTIR spectra of 12 different alkali activated façade panels cured at room temperature for three days, followed by three days of curing at 60° C.

Source: own.

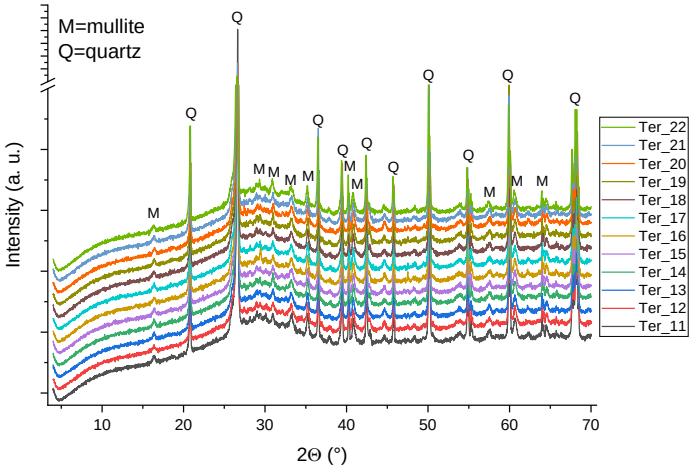

Figure 9: X-ray diffraction patterns of 12 different alkali activated façade panels cured at room temperature for three days followed by three days at 60 °C.

Source: own.

12 different X-ray diffraction patterns of alkali-activated façade panels are shown in Figure 9. The amount of amorphous content is around 80 wt% in all the samples (an amorphous halo is observed at the same position in all samples between 22° in 38°). Crystal phase, representing about 20 wt% of all panel material, is primarily consisted of mullite and quartz.

The leaching results of toxic elements from 12 randomly selected façade panels are presented in Table 5. Most of the elements are below the upper limits for inert waste (concentrations of elements measured in the samples are shown in Table 5, and the requirements are provided in Table 6). Cr, As and Sb exceeded this limit in some cases, however, while Mo was above the limit in all cases. Cu did not exceed the limit values set by the Decree on Waste Landfill, but Slovenian regulations are slightly stricter when waste material is intended for recycling, meaning the leached concentrations of Cu are above the values permitted within Slovenia.

Table 5: Concentrations of toxic metals from 12 different façade panels. Concentrations coloured in red are above the limits stated in the Decree on Waste Landfill, whereas the values in blue show the concentrations of elements that exceeded the required values outlined in the Decree on Waste.

Element (mg/kg)	Cr	Co	Ni	Cu	Zn	As	Se	Mo	Cd	Sb	Ba	Hg	Pb
Ter_11	0.54	0.01	0.23	0.64	0.09	0.59	0.06	1.16	0.002	0.05	0.13	0.005	0.11
Ter_12	0.56	0.02	0.34	0.98	0.05	0.47	0.06	1.09	0.001	0.03	0.11	0.004	0.04
Ter_13	0.48	0.02	0.30	1.19	0.04	0.45	0.06	0.95	0.001	0.04	0.07	0.004	0.05
Ter_14	0.50	0.01	0.23	0.47	0.02	0.55	0.06	1.04	0.001	0.04	0.08	0.003	0.03
Ter_15	0.40	0.02	0256	1.00	0.01	0.39	0.04	0.72	0.001	0.04	0.07	0.004	0.04
Ter_16	0.51	0.01	0.31	0.87	0.03	0.27	0.04	0.89	<0.001	0.02	0.05	0.004	0.05
Ter_17	0.46	0.01	0.26	0.82	0.02	0.30	0.04	0.91	<0.001	0.02	0.05	0.003	0.03
Ter_18	0.39	0.02	0.17	0.41	0.05	0.32	0.04	0.90	<0.001	0.03	0.08	0.003	0.04
Ter_19	0.37	0.02	0.19	0.92	0.03	0.34	0.04	0.92	0.001	0.04	0.05	0.003	0.06
Ter_20	0.38	0.02	0.22	0.77	0.01	0.47	0.04	0.82	<0.001	0.04	0.06	0.003	0.02
Ter_21	0.42	0.01	0.22	0.83	0.02	0.37	0.04	0.75	<0.001	0.04	0.06	0.003	0.04
Ter_22	0.51	0.01	0.22	0.58	0.05	0.64	0.04	0.93	<0.001	0.12	0.20	0.004	0.08

A comparison was also made between the leaching of elements from the façade panel prepared from mix design 1 and that prepared using the current formula (mix design 3), which shows a decrease in the concentrations of most of the toxic elements (Table 7). Significant decreases are observed in the case of Cu and Mo. The addition of a smaller amount of sodium silicate, and the absence of NaOH, could lead to a slight reduction in the pH of the solution, which could influence the leaching potential of these two elements. However, curing conditions at 60 °C

instead of room temperature may also improve the immobilisation of those two elements (Izquierdo et al., 2010; Keulen et al., 2018).

Table 6: The concentrations of inert and non-hazardous waste that should not be exceeded according to the Decree on Waste Landfill, and the limit on elemental concentrations that can be used in recycled products based on data from the Slovene Decree on Waste.

Element (mg/kg)	Cr	Co	Ni	Cu	Zn	As	Se	Mo	Cd	Sb	Ba	Hg	Pb
Inert waste	10.0	/	10.0	50.0	50.0	2.0	0.5	10.0	3	0.7	100.0	0.20	10.0
Non-hazardous waste	0.5	0.03	0.4	0.5	2.0	0.1	0.6	0.5	0.025	0.3	5.0	0.005	0.5
Decree on waste (SLO)	0.5	/	0.4	2.0	4.0	0.5	0.1	0.5	0.04	0.06	20.0	0.01	0.5

Table 7: A comparison of the toxic metals leached from the final mix design (mix design 3) and the first mix developed in the lab. The concentrations coloured in red are above the required values stated in the Decree on Waste Landfill, whereas the values in blue are the elemental concentrations that exceeded the values required according to the Decree on Waste.

Element (mg/kg)	Cr	Co	Ni	Cu	Zn	As	Se	Mo	Cd	Sb	Ba	Hg	Pb
Mix design 1	0.65	0.04	0.83	2.60	0.15	0.54	0.16	1.69	0.003	0.04	0.25	0.005	0.09
Mix design 3	0.46 ± 0.10	0.015 ± 0.005	0.25 ± 0.05	0.79 ± 0.23	0.04 ± 0.02	0.43 ± 0.12	0.05 ± 0.01	0.92 ± 0.13	0.0008 ± 0.0004	0.04 ± 0.02	0.08 ± 0.04	0.004 ± 0.001	0.05 ± 0.02

3 Conclusions

The façade panels prepared varied in terms of their mechanical properties as a result of the unevenly milled batches of (pre-milled) mineral wool. If a higher proportion of smaller fractions are present in the mixture, the mechanical properties are better. There is, however, no correlation between the mechanical properties of the panels and the degree of polymerization, open porosities and the leaching parameters – an improvement in mechanical properties does not necessarily lead to an improvement in the immobilization of elements, as other processes, such as diffusion and dissolution, may affect the leaching of elements. With a slight modification to the mix design and a change in the curing conditions, the leached concentrations of most

toxic elements were reduced. This is significantly important for Cr, Ni, Cu, As, Se, Mo and Hg, all of which exceeded the permitted values outlined in the Decree on Waste Landfill and the Decree on Waste. Additional modifications to the mix design and curing process should, however, be tested, in order to reduce the concentrations of those elements to below the limit values required for recycled products. Further work with respect to the composition of samples is, however, needed, to ensure the mixture is suitable for use as a commercially-available recycled product.

Acknowledgments

This project has received funding from the European Union's EU Framework Programme for Research and Innovation, Horizon 2020, under Grant Agreement #821000. We acknowledge financial support from the Slovenian Research Agency, Slovenia, through project No. Z2-3199 »The immobilisation and leaching of toxic trace elements in alkali-activated materials prepared from locally available waste and by-products«.

References

Garcia-Lodeiro, I., Palomo, A., Fernández-Jiménez, A., Macphee, D.E., 2011. Compatibility studies between N-A-S-H and C-A-S-H gels. Study in the ternary diagram Na2O–CaO–Al2O3–SiO2–H2O, Cem. Concr. Res. 41, 923-931.
https://doi.org/https://doi.org/10.1016/j.cemconres.2011.05.006.

Izquierdo, M., Querol, X., Phillipart, C., Antenucci, D., Towler, M., 2010. The role of open and closed curing conditions on the leaching properties of fly ash-slag-based geopolymers, J. Hazard. Mater.176, 623-628.

Keulen, A., van Zomeren, A., Dijkstra, J.J., 2018. Leaching of monolithic and granular alkali activated slag-fly ash materials, as a function of the mixture design, Waste Manag. 78, 497-508.
https://doi.org/https://doi.org/10.1016/j.wasman.2018.06.019.

Kinnunen, P., Yliniemi, J., Talling, B., Illikainen, M., 2017. Rockwool waste in fly ash geopolymer composites, J. Mater. Cycles Waste Manag. 19, 1220-1227.
https://doi.org/10.1007/s10163-016-0514-z.

Kowatsch, S., 2010, Mineral Wool Insulation Binders BT - Phenolic Resins: A Century of Progress, en: L. Pilato (Ed.), Springer Berlin Heidelberg, Berlin, Heidelberg: p. 209-242.
https://doi.org/10.1007/978-3-642-04714-5_10.

Müller, A., Leydolph, B., Stanelle, K., 2009. Recycling Mineral Wool Waste: Technologies for the Conversion of the Fiber Structure, Part 1, Interceram. 58, 378-381.

Official Gazette of Republic Slovenia, 2014. Decree on Waste Landfill, Nos. 2020, 10/14, 54/15, 36/16, 37/18. https://www.ecolex.org/details/legislation/decree-on-the-landfill-ofwaste-lex-faoc130542/.

Pavlin, M., Horvat, B., Frankovič, A., Ducman, V., 2021a. Mechanical, microstructural and mineralogical
evaluation of alkali-activated waste glass and stone wool, Ceram. Int.
https://doi.org/https://doi.org/10.1016/j.ceramint.2021.02.068.

Pavlin, M., Horvat, B., Ducman, V., 2021b. Challenges at upscaling from laboratory to industrial level in Wool2Loop project, en: Technol. Bus. Model. Circ. Econ., Portorož (Slovenia), p. 35. http://tbmce.um.si/wp-content/uploads/2021/09/02_TBMCE2021_Book_of_Abstracts.pdf.

Pavlin, M., Horvat, B., Ducman, V., 2022. Preparation of façade panels based on alkali-activated waste mineral wool, their characterization and durability aspects, Int. J. Appl. Ceram. Technol. n/a. https://doi.org/https://doi.org/10.1111/ijac.13998.

Väntsi, O., Kärki T., 2014. Mineral wool waste in Europe: A review of mineral wool waste quantity, quality, and current recycling methods, J. Mater. Cycles Waste Manag. 16, 62-72. https://doi.org/10.1007/s10163-013-0170-5.

Yliniemi, J., Kinnunen, P., Karinkanta, P., Illikainen, M., 2016. Utilization of Mineral Wools as Alkali-Activated Material Precursor, Materials (Basel). 9, 312. https://doi.org/10.3390/ma9050312.

Yliniemi, J., Walkley, B., Provis, J.L., Kinnunen, P., Illikainen, M., 2020. Nanostructural evolution of alkaliactivated mineral wools, Cem. Concr. Compos. 106, 103472. https://doi.org/10.1016/J.CEMCONCOMP.2019.103472.

Yu, P., Kirkpatrick, R.J., Poe, B., McMillan, P.F., Cong, X., 1999. Structure of Calcium Silicate Hydrate (C-S-H): Near-, Mid-, and Far-Infrared Spectroscopy, J. Am. Ceram. Soc. 82, 742-748. https://doi.org/10.1111/j.1151-2916.1999.tb01826.x.

RECYCLABILITY OF RECYCLED CONCRETE PRODUCTS IN CEMENTS

SANTIAGO ROSADO,[1] LIDIA GULLÓN,[1] LETICIA PRESA,[2] JAIME MORENO[3]

[1] Fundación Gómez Pardo, Madrid, Spain
santiago.rosado@fgomezpardo.es, direccion.tecnica@fgomezpardo.es
[2] Universidad Politécnica de Madrid, Escuela Técnica Superior de ingenieros de Minas y Energía, Madrid, Spain
leticia.presa.madrigal@upm.es
[3] Tecnalia Research & Innovation, Basque Research and Technology Alliance (BRTA), Astondo Bidea, Derio, Spain
jaimemoreno@tecnalia.es

Abstract This research addresses the recycling possibilities of a concrete product that contains coarse concrete aggregate as recycled material. The use of this finely milled product is proposed as an active addition to cement that already includes by-products in their composition. The partial substitution of cement by secondary raw materials contributes positively to the reduction of waste dumping and to the reduction of greenhouse gas emissions. However, the substitution rates of secondary raw materials are higher in concrete aggregates (20%) than in cements. The dosage of a concrete includes approximately three times more coarse aggregate than cement. This means that the amount of waste that can be incorporated into recycled concrete is greater if it is done as coarse aggregate than if it is added to cement. The main advantage of the partial substitution of cement lies in the reduction of CO_2 derived from the decarbonization process of the cement raw materials.

Keywords: circular economy, cement, concrete, recycling, secondary raw material

University of Maribor Press

DOI https://doi.org/10.18690/um.fkkt.1.2023.4
ISBN 978-961-286-692-1

1 Introduction

The use of concrete wastes in new building products in the Circular Economy framework currently has a medium scope. On one hand, there are already industrial applications of recycled concrete aggregates to be used in new concretes. But on the other hand, the researches about how to use this waste as fine aggregate in mortar or concrete or finely milled as cement addition is still under development.

It is needed to focus on recycled concrete because now the standard (AEN/CTN 146) allows to include until a 20 % of coarse aggregate from recycled aggregates. However, the Circular Economy concept requires to consider the recyclability of these new products one they are at the end of their live and when they are considered as wastes.

One recycling way of these wastes is the treatment in order to manufacture again recycled aggregates to be added to new concrete mixes. On this way, the new concrete will include a 20 % of recycled concrete. But this already included a 20 % of recycled concrete. So, it means, in total a 24 % of recycled material so in according to that standard, the proportion of recycled material will increase in each step. Although it will be limited due to the technical characteristics.

The second recycling way is the use in cement. If it is considered the Portland Cement production in Europe in the last years has passed 100 million tons per year, even short addition may have a huge impact. In fact, the waste additions to cement is already a common practice but to add other options may be of great interest because now some of these wastes are sold as raw materials with a high dependence and a high availability risk. In addition, it is necessary to consider that the cement industry is responsible of the 5 of the greenhouse gases produced every year (Benhelal, Shamsaei et al. 2021) and the 5-8 % of the CO_2 emissions (Sousa, Bogas 2021). Therefore, to include low proportions of secondary raw materials as cement additions will positively contribute to decrease these emissions. It is due to the main chemical process associated to the cement manufacturing: the decarbonization. Calcium carbonate present in the cement is transformed into calcium oxide with the emission of CO_2. So, if other compounds different than the calcium carbonate are used in cements, the emissions will decrease.

The possibility to use concrete waste as cement addition depend on the state of the waste in terms of particle size. It is important to use the reactivity of the dust (<0,063 mm) which is obtained by a milling of the concrete, in order to perform partial substitutions of the cement (Xiao, Ma et al. 2018). However, it seems difficult to perform cements additions higher than 10 % due to the strength decrease of the final products. In addition, it must be considered that these additions should be combined with those commonly used now such as fly ashes or silica fumes which have already high performance.

This work aims to analyse the possibility of use waste from recycled concrete as active addition to an industrial cement in order to evaluate the potential advantages and the limits of use. The plan is to evaluate short additions of milled concrete in cements: 5, 7 and 10 %. Although the potential reduction of the CO_2 is about 38-76 kg per ton of produced cement, the final strength of the cement should be tested.

2 Materials

The concrete waste used in this study comes from the manufacturing of concrete probes with a 20 % of recycled concrete aggregate. The wastes of the compressive strength tests from a previous research which included a new concrete with recycled material are studied in the present work. The compressive strength of this old concrete at 28 days was 34,3 Mpa and it was manufactured with:

- CEM II/A-M 42,5 R.
- Coarse aggregate 6/20 mainly composed by silica.
- A substitution of 20 % of the coarse aggregate by recycled concrete aggregate from a CDW manager located in Madrid
- Fine aggregate 0/6 mainly composed by silica.
- Superplasticiser
- Water

The cement used in the present research is the same than the used in the previous one: CEM II/A-M 42,5 R. A Portland Cement with the addition of fly ashes and limestone (12-20 %) and with a compressive strength at 28 days of 42,5 Mpa.

3 Method

The CO_2 emissions have been estimated in a theoretical way. Assuming a minimum proportion of calcium oxide present in the cement. And considering that all this oxide comes from calcium carbonate after a decarbonisation treatment in a specific proportion which depends of the stoichiometric ratio.

$$CaCO_3 \rightarrow CaO + CO_2$$

In the behaviour of the additions has been considered the main composition of them:

- Fly ashes: no calcium carbonate
- Milled concrete: no calcium carbonate
- Limestone: a 100 % of calcium carbonate.

4 Discussion

The main source of CO_2 pollution by the cement production process comes from the decarbonisation of the lime in (calcium carbonate) into calcium oxide by the thermal treatment of the raw materials:

$$CaCO_3 \rightarrow CaO + CO_2$$

It is possible to consider a typical minimum content of CaO in cement of 60 % which means a theoretical emission of 765 kg of CO_2 per ton of produced cement. Although this value may change with the temperature of the process and the energetic consumption of fuel has been not considered. A substitution of 5-10 % of cement per milled concrete (already decarbonized) may reduce about 38-76 kg of CO_2 per ton of produced cement.

There is a natural carbonisation of the concrete during their live so in real terms there will be a small amount of calcium carbonate in the concrete wastes. However, it is not easy to measure this parameter in concrete wastes since it depends on the

type of original concrete, its age and weather conditions, among others. For this research, no natural carbonisation of the concrete has been considered.

The cement of this study contains about 12-20 % of fly ashes and limestone so its emissions may be partially reduced if this proportion are completely fly ashes (which do not include carbonate) but in the case of a predominance of limestone as active addition the emissions will be higher than a cement without this kind of addition.

Although the current trend is the addition of limestone after the thermal process (and therefore without the emission of CO_2), there is a greater tendency towards the calcination of secondary raw materials in order to achieve their activation. Because the second recycling of the products will not only contain cement, but also other waste such as ceramic or concrete, the calcination of this cement will emit CO_2 from both cement and the limestone. Therefore, all additions before the thermal process have been considered.

It is possible to consider six different scenarios where the addition is minimum (12%) and with three different ratios fly ashes / limestone:

- 100 % limestone / 0% fly ashes
- 50 % limestone / 50 % fly ashes
- 0 % limestone / 100 % fly ashes

And the same three scenarios assuming the highest addition (20%).

- 100 % limestone / 0% fly ashes
- 50 % limestone / 50 % fly ashes
- 0 % limestone / 100 % fly ashes

The next table summarise this situation and shows the theoretical emissions in kg per ton of produced cement.

Table 1: Theoretical CO_2 emissions (kg) per ton of produced cement (CEM II).

	Clinker (%)	Fly ashes (%)	Limestone (%)	Clinker emissions (kg/t)	Limestone emissions (kg/t)	Cement emissions (kg/t)
	100	0	0	765	0	765
1	88	0	12	672,8	152,9	825,7
2	88	6	6	672,8	76,5	749,2
3	88	12	0	672,8	0,0	672,8
4	80	0	20	611,6	254,8	866,5
5	80	10	10	611,6	127,4	739,0
6	80	20	0	611,6	0,0	611,6

As it was expected, the limestone addition have a worse effect in terms of emissions than the original cement without addition (equivalent to CEM I). But the addition of fly ashes is very positive even in the case of use the same proportion of fly ashes than limestone.

These results can be optimized with the addition of milled concrete waste in a proportion of 5, 7 or 10 % of the total cement. They are small quantities that will not negatively affect to the final strength of the products or even can improve it. The next table shows a theoretical estimation of those additions.

Table 2: Theoretical CO_2 emissions (kg) per ton of CEM II with milled concrete produced cement (CEM II with commercial additions and milled concrete)

	Clinker (%)	Fly ashes (%)	Limestone (%)	Clinker emissions (kg/t)	Limestone emissions (kg/t)	Cement emissions (kg/t)	Cement emissions (kg/t)- Concrete (5%)	Cement emissions (kg/t)- Concrete (7%)	Cement emissions (kg/t)- Concrete (10%)
	100	0	0	765	0	765			
1	88	0	12	672,8	152,9	825,7	784,4	767,9	743,1
2	88	6	6	672,8	76,5	749,2	711,8	696,8	674,3
3	88	12	0	672,8	0,0	672,8	639,1	625,7	605,5
4	80	0	20	611,6	254,8	866,5	823,1	805,8	779,8
5	80	10	10	611,6	127,4	739,0	702,1	687,3	665,1
6	80	20	0	611,6	0,0	611,6	581,0	568,8	550,5

In the best scenario (6), a substitution of 10 % of milled concrete by cement with a 20 % of fly ashes can reduce the emission above 30 %. In the most common cases (scenario 5) where a mix of lime and fly ashes are used, the reduction may be about 7-13 % depending the quantity of milled concrete added.

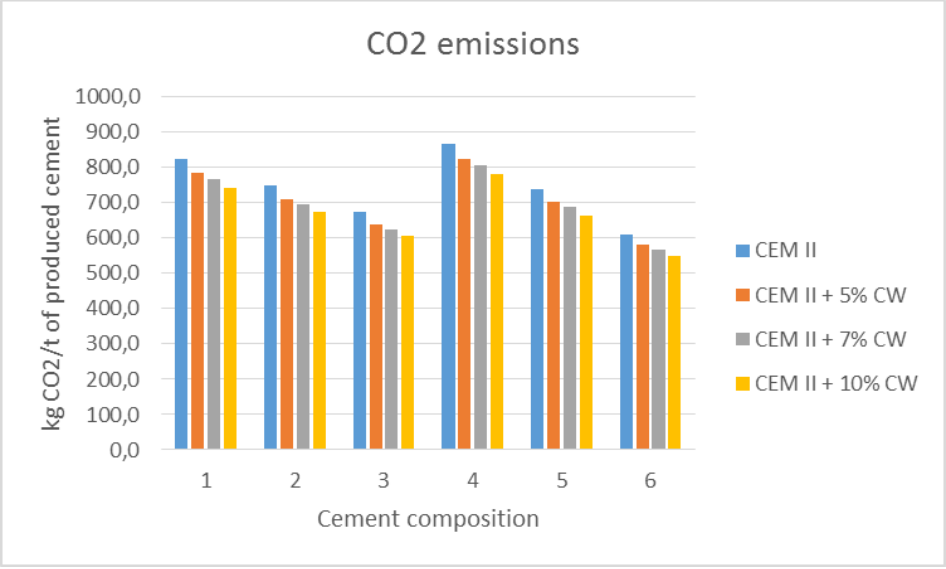

Figure 1: CO_2 emissions by every kind of addition.
Source: own.

The highest reduction of the CO_2 emissions are according to the highest additions of the milled concrete. The main issue to be solved is the mechanical performance of these kind of cement additions. Probably the limit proportion is 10 %. Additions higher than this may cause a decrease of the strength. But lower proportions such as 7 % may develop a high strength, even improving the strength of the original cement. But it depends of the quality of the concrete waste. In general terms, if the presence of sulphates is low, the quantities of silica and calcium oxide are high, the final strength may be optimum. But in any case, to perform a detailed strength study is required.

5 Conclusions

In a theoretical framework, the milled concrete addition to commercial cements in low proportions (5, 7 and 10 %) may considerably improve the CO_2 emissions due to the decarbonisation of calcium carbonate into calcium oxide. In addition, if the cement to be used already includes other additions such as fly ashes or limestone, the potential reduction of those emissions is interesting (7-13 %).

With this forecast of emissions saving, it is suggested to continue the research with a practical study whose main goal should be to define the maximum proportion of milled concrete which is possible to use in this kind of cement. A simple test plan should include a reference sample without additions and mixes with additions of 5, 7 and 10 % of milled concrete in order to study the final strength at 7, 28 and 90 days. On this way, the potential pozzolanic activity of the materials (fly ashes are considered as pozzolanic material) will be also studied.

Acknowledgement

The authors thank the Fundación Gómez Pardo for its support to the research and development of this publication.

Funding

This article has been partially funded by Cinderela project which has received funding from the European Union's Horizon 2020 research and innovation Programme under grant agreement Nº776751.

References

AEN/CTN 146, *UNE-EN 12620 Áridos para hormigón.*

BENHELAL, E., SHAMSAEI, E. and RASHID, M.I., 2021. Challenges against CO2 abatement strategies in cement industry: A review. *Journal of Environmental Sciences,* 104, pp. 84-101.

SOUSA, V. and BOGAS, J.A., 2021. Comparison of energy consumption and carbon emissions from clinker and recycled cement production. *Journal of Cleaner Production,* 306, pp. 127277.

XIAO, J., MA, Z., SUI, T., AKBARNEZHAD, A. and DUAN, Z., 2018. Mechanical properties of concrete mixed with recycled powder produced from construction and demolition waste. *Journal of Cleaner Production,* 188, pp. 720-731.

CATALYZED DEGRADATION OF POLYETHYLENE TEREPHTHALATE

ŽIGA SAMSA, DARJA PEČAR, ANDREJA GORŠEK

University of Maribor, Faculty of Chemistry and Chemical Engineering Maribor, Slovenia
ziga.samsa@student.um.si, darja.pecar@um.si, andreja.gorsek@um.si

Abstract In this research catalyzed degradation of polyethylene terephthalate was performed. For that purpose, ZSM-5 zeolite was synthesized as an acid catalyst. For its characterization N_2 adsorption, scanning electron microscopy, NH_3 temperature programmed desorption, differential scanning calorimetry, thermogravimetric analysis, dynamic light scattering, and Fourier transform infrared spectroscopy were utilized. Degradation reactions were performed in high pressure crucibles using differential scanning calorimeter at different temperatures (200, 250 and 300) °C and time intervals (2.5, 5, 10 and 15) min. Samples were analyzed using high performance liquid chromatography coupled with UV-VIS detector. The results revealed that the highest conversion was achieved at 300 °C and 10 min. The analysis of obtained results showed that despite the differences in conversions being not as high as expected, reactions with the catalyst were slightly more effective than without it. For the future work, we plan to finetune the synthesis procedure to obtain more active catalyst. And for the upgrade of the study the kinetic analysis of the reaction will be conducted.

Keywords:
degradation, catalyst, ZSM-5, polyethylene terephthalate, DSC

University of Maribor Press

DOI https://doi.org/10.18690/um.fkkt.1.2023.5
ISBN 978-961-286-692-1

1 Introduction

Polymers represent materials, which we use daily practically everywhere in our lives. Their usage in food, cosmetics, building and electro industry has risen significantly in the past decades. (Namazi, 2017)

Life without synthetic materials is not imaginable. Population growth, higher life standard and the revolution of technology are the reasons for high production of polymers. Most of the produced plastic and polymer products are not biodegradable, which has a significant impact on the environmental pollution. Researchers are looking for an economical, technological and environmental solution for a replacement of polymer materials and its recycling or transformation to other useful products. (Manfra, 2021 and Kumar Gupta, 2022)

Polyethylene terephthalate (PET), which belongs to the polyester family, is a widely used linear semi-crystalline thermoplastic polymer due to its favorable mechanical and thermal properties. It belongs to the unbranched polymers obtained by the esterification reaction between ethylene glycol (EG) and terephthalic acid (TPA) or by trans-esterification between ethylene glycol and dimethyl terephthalate. Due to its advantages and useful properties (flexibility, recyclability, electrical-insulating properties, high mechanical strength, low weight, resistance to alcohols and aliphatic hydrocarbons), it is commercially found mainly in packaging, fibers and electronics. It is more suitable for recycling compared to other alternative materials. The most used recycling methods are hydrolysis and mechanical mixing. In chemical recycling, TPA and EG are formed as hydrolysis products. From an economic and environmental point of view, mechanical recycling is more often used. (PET, 2022 and Yan, 2023)

The aim of this study was to synthesize a new acid catalyst, which would be appropriate for PET degradation. Advanced analytical techniques were used for catalyst characterization.

2 Materials and methods

2.1 Materials

All the reagents and solvents used were of analytical grade. Sodium hydroxide (NaOH, 99 %), Sodium aluminate ($NaAlO_2$, Al_2O_3: 50-56 %, Na_2O: 37-45 %), Tetrapropylammonium bromide (TPABr, 98 %), Bis(2-hydroxyethyl) terephthalate (BHET), *Trifluoroacetic acid* (TFA, 99 %) were purchased from Sigma-Aldrich, Ammonium nitrate (NH_4NO_3, 99 %) from Kemika, Tetraethyl orthosilicate (TEOS, 98 %) from J&K Scientific Ltd., Polyethylene terephthalate (PET) from Melanin, and Acetonitrile (ACN 99,9 %) from Honeywell.

2.2 Methods

2.2.1 Catalyst synthesis

0.05 g of $NaAlO_2$ and 0.6 g of NaOH were dissolved in 101.25 mL of deionized water. 2.1 g of TPABr and 6.425 g of TEOS were added to the solution and stirred overnight. Then the solution was transferred into an autoclave and aged for 48 h at 180 °C. Afterwards, the solution was filtered, solid product washed with deionized water, dried at 100 °C and then calcined for 6 h at 550 °C. Ion exchange of solid product was performed with 500 mL of 0.2 M NH_4NO_3 solution during stirring for 3 h at 80 °C. The particles were filtered and dried. The process of ion exchange was repeated three times. At the end the solid product was calcined for 6 h at 550 °C.

2.2.2 Catalyst characterization

The synthesized catalyst was characterized by nitrogen adsorption-desorption (BET), Fourier transform infrared spectroscopy (FTIR), scanning electron microscopy (SEM), dynamic light scattering (DLS), thermogravimetric analysis (TGA), and temperature programmed desorption (TPD).

2.2.3 Polyethylene terephthalate degradation

Polyethylene terephthalate degradation reactions were performed in a differential scanning calorimeter from Mettler Toledo (DSC3). The reactions were carried out in a small high- pressure stainless-steel reactor with a volume of 30 µL, at temperatures 200, 250 and 300 °C and time 2.5, 5, 10 and 15 min. At each temperature and time, the reaction was performed with and without the catalyst. 5 mg of polyethylene terephthalate (PET) and 2.5 mg of the ZSM-5 catalyst were weighed into the reactor. Then 20 µL of deionized water was added. The reactor used for PET degradation reaction is shown in Figure. After a certain time, 10 µL of the sample was withdrawn from the reactor and diluted with 490 µL of mobile phase. It was further used for the analysis.

Figure 1: High-pressure stainless-steel reactor with the sample.
Source: own.

2.2.4 Analysis

The analyses of TPA and intermediate BHET were performed on a Hewlett Packard series 1100 high performance liquid chromatograph HPLC coupled to a UV-VIS detector. The separation of compounds was performed on an Agilent Eclipse XD8-C18 chromatography column (4.6 x 250 mm, 5 µm) at 30 °C. The mobile phase consisted of two solvents, A: acetonitrile (ACN) and B: water (0.1 % TFAA), (A:B=25:75). The flow rate through the column was 1 mL min^{-1}. The detection was performed at 240 nm. The samples were washed from reactor with 0,5 % NaOH and diluted to 2 mL. This solution

was then further diluted (50 µL of sample and 1450 µL of mobile phase) and filtered through a 0.22 µm PES filter. The TPA and intermediate BHET concentrations were obtained from calibration curves.

3 Results and discussion

3.1.1 Catalyst characterization

The nitrogen adsorption/desorption isotherms (Figure 2) of the catalyst show type IV isotherms with a clear hysteresis loop at relative pressures of p/p_0 = (0.3 – 1.0). The determined BET surface area was 360.6 m^2/g, pore size 2.0 nm and pore volume 0.18 cm^3/g. The synthesized catalyst belongs to mesoporous material with a relatively large surface area.

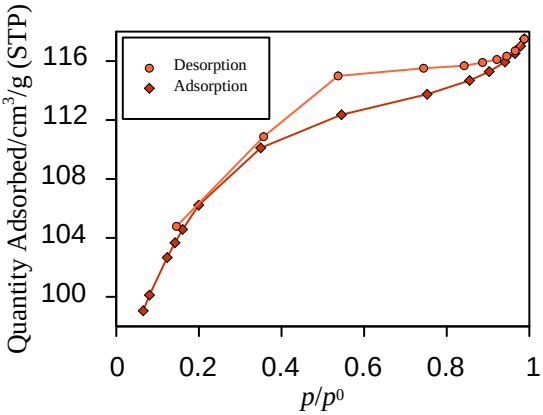

Figure 2: BET.
Source: own.

From the FTIR spectra it was not possible to determine the presence of specific functional groups.

The morphology of the synthesized catalyst was observed by scanning electron microscopy (SEM) and the images obtained are shown in Figure 3. We can see that the catalyst forms clusters of several smaller particles. From higher magnifications it can be seen that the size of one particle is about 0.5 µm, which is in agreement with DLS measurement, where the average particle size was determined to be 0.57 µm.

From the results of the TGA measurement we could determine only one step change at the beginning of the measurement to around 200 °C, which is attributed to the loss of bound water.

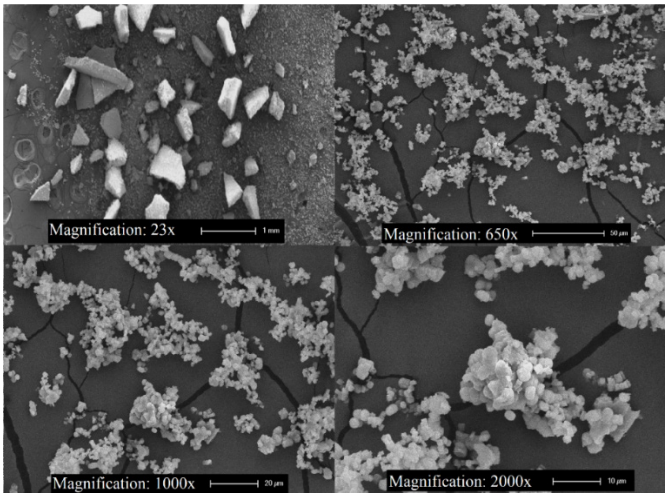

Figure 3: SEM image of ZSM-5 catalyst.
Source: own.

In order to determine the acid properties of synthesized catalyst temperature programed desorption of NH_3 was performed. From the response (Figure 4) it is clear that there are manly weak acid sites presented (peak around 120 °C) and only few strong acid ones (peak around 450 °C).

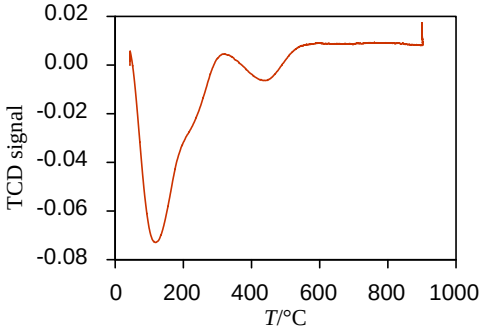

Figure 4: TPD of NH_3.
Source: own.

3.1.2 Polyethylene terephthalate degradation

The reactions of PET degradation were performed at different temperatures (200, 250 and 300 °C) and time periods (2.5, 5, 10 and 15 min). The obtained concentrations of TPA and BHET at 200 °C are shown in Figure 5.

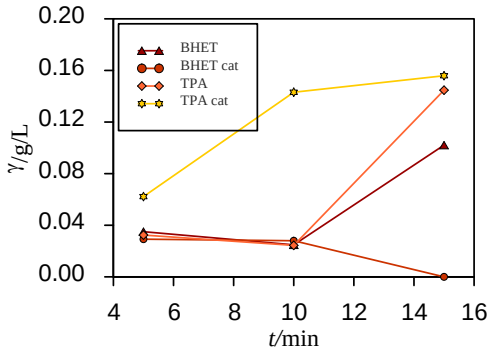

Figure 5: Concentrations of TPA and BHET regarding time at 200 °C.
Source: own.

It is known that during the degradation of PET two intermediates BHET and MHET are first formed and then the degradation proceeds towards to TPA. Because of the inaccessibility of MHET we were only able to determine the concentrations of BHET and TPA. We observed that at all temperatures the concentrations of TPA and BHET increase with increasing time of the reaction. But the increase in the concentrations is more pronounced with increasing temperaturej. We also confirmed that the synthesized solid acid catalyst was active during the degradation of PET. Namely, for most reactions performed with the catalyst the concentrations of formed TPA were higher than for those without the catalyst.

4 Conclusion

The reactions of PET degradation took place in a differential scanning calorimeter. Further, the catalyst characterization using different characterization methods was performed. It was confirmed that synthesized catalyst has acid properties. The reaction with a catalyst was more effective at a certain temperature than without it, yet the achieved conversions were lower than expected. The conclusion drawn from this study is that

synthesized catalyst is not efficient enough to be used in the degradation of polyethylene terephthalate. In the comparison between the use of the catalyst and the increase of the reaction temperature, it was found that in our case the temperature has a greater influence on the reaction conversion.

Acknowledgments

We would like to thank the Slovenian Research Agency (ARRS) for co-financing the research project "Planning and management of sustainable value chains of the production of plastic materials for the transition to a circular economy" with the code J7-3149.

References

Kumar Gupta, R., Guha, P. and Prakash Srivasta, P. (2022). Natural polymers in bio-degradable/edible film: A review on environmental concerns, cold plasma technology and nanotechnology application on food packaging- A recent trends. *Food Chemistry Advances*, *1*, 100135. https://doi.org/10.1016/j.focha.2022.100135.

Manfra, L., Marengo, V., Libralato, G., Costantini, M., De Falco, F. and Cocca, M. (2021) Biodegradable polymers: A real opportunity to solve marine plastic pollution?. *Journal of Hazardous Materials*, 416, 125763. https://doi.org/10.1016/j.jhazmat.2021.125763.

Namazi, H. (2017). Polymers in our daily life. *Bioimpacts*, *7*, 73–74. https://doi.org/10.15171/bi.2017.09.

PET Plastic (Polyethylene Terephthalate): Uses, Properties & Structure, (n.d.). https://omnexus.specialchem.com/selection-guide/polyethylene-terephthalate-pet-plastic (accessed June 26, 2022)

Yan, M., Yang, Y., Shen, T., Grisdanurak, N., Pariatamby, A., Khalid, M., Hantoko, D. and Wibowo, H. (2023). Effect of operating parameters on monomer production from depolymerization of waste *polyethylene terephthalate* in supercritical ethanol. *Process Safety and Environmental Protection*, *169*, 212–219. https://doi.org/10.1016/j.psep.2022.11.011.

ELECTROCOAGULATION IMPLEMENTATION FOR TEXTILE WASTEWATER TREATMENT PROCESSES

MARJANA SIMONIČ
University of Maribor, Faculty of Chemistry and Chemical Engineering Maribor, Slovenia
marjana.simonic@um.si

Abstract Electrocoagulation (EC) has been employed recently to treat tannery, textile, and coloured wastewater. Three main processes are gathered in EC process, namely electrochemistry, coagulation, and flotation. This technique uses DC currents source between metal electrodes immersed in the textile effluent, which causes the dissolution of electrode plates into the effluent. The main advantage of EC compared to chemical coagulation technique is that EC generates less sludge. The objective of the present manuscript is to review the potential of electrocoagulation for the treatment of textile effluent. The most influential factors on removal efficiency, such as initial pH, time of EC, conductivity, current density, initial dye concentration and periodically reversal current on electrodes were discussed. Considering the circular economy concept, which focuses on positive society-wide benefits, manufacturing brick or ceramic materials is feasible method for disposing sludge.

Keywords:
electrocoagulation,
textile effluent,
metal removal,
costs,
current density

University of Maribor Press

DOI https://doi.org/10.18690/um.fkkt.1.2023.6
ISBN 978-961-286-692-1

1 Introduction

The effluents from textile industry as well as tannery are heavily polluted with heavy metals, such as chromium, and different types of organic matter, especially dyes. The water is dark coloured and does not allow the passage of sun light, therefore, it might be toxic and poorly chemical and biological degradable. (Moussa et al, 2017) Due to toxicity of dyes and metals in textile water, biological treatment is insufficient (Emamjomeh and Sivakumar, 2009).

Chemicals are added to physically remove during traditional techniques such as coagulation or adsorption on traditional adsorbents such as activated carbon in used. In both cases a lot of sludge is generated. Therefore, electrocoagulation (EC) has been employed to treat among other also tannery, textile, and coloured wastewater. The process generates no additional chemicals. In the literature (Mousssa et al, 2017) it was stated that more than hundred years electrocoagulation has been applied to remove pollutants from different types of industrial wastewater, such as: emulsion wastewater, coloured wastewater (textile), pulp and paper industry wastewater, tannery, and also from food industry. EC and other electrochemical wastewater treatment processes are considered as an environmentally friendly technology. (Mousssa et al, 2017)

Heavy metals, such as Chromium, is very toxic, even carcinogenic as Cr(VI). The Cr removal dynamics was explained (Espinoza et al, 2009). The positive chromium ions are neutralized after movement to the ferrous ions at anode under the electric field, and Cr-ions electrical charge is neutralized. After 15 min, a 93 % drop in Cr concentration was measured as a consequence of the particle coagulation. The electrolysis time of 1 hour was enough for the almost total neutralization of Cr-ions.

The aim of present study was to identify the current state of the EC and review of recent advances in the field of EC. Also ECs' potential as an effective textile wastewater treatment method was considered. From the circular economy concept, disposing sludge could be used as secondary material for manufacturing brick or ceramic materials (Sandoval et al, 2021).

2 Methods

At the iron anode the chemical oxidation to Fe^{2+} take place (Chen, 2004).

Next reaction at pH above 7:

$$Fe^{2+} + 3OH^- \rightarrow Fe(OH)_2^- \quad (1)$$

And at pH below 7:

$$Fe^{2+} + O_2 + 2H_2O \rightarrow 4Fe^{3+} + 4OH^-. \quad (2)$$

and

$$Fe^{3+} + 3OH^- \rightarrow Fe(OH)_3, \quad (3)$$

From water oxygen and H+ ions are produced.

At the iron cathode hydrogen is produced:

$$2H_2O + 2e^- \rightarrow H_2 + 2OH^- \quad (4)$$

Beside monomeric also polymeric species could form, e.g. $Fe(H_2O)_6^{3+}$, $(OH)_2^+$, $Fe_2(H_2O)_8\,(OH)_2^{4+}$and $Fe(H2O)_6\,(OH)_4^{4+}$ $Fe(H2O)_5$ if pH changes (Hendaoui et al, 2018).

NaCl increases the production rate of such polymeric species. In textile industry a lot of dyes arre present in water. (Eq.5-6) (Nandi and Patel, 2017):

Dye+ Fe(monomeirc) → monomeric-komplex (s) (5)
Dye+ Fe(polymeirc) → polymeric-komplex (s) (6)

In the second step the adsorption take place, following reactions 7 and 8:

komplex + $Fe_n(OH)_{n\,(s)}$ → sludge (7)
Dye + $Fe_n(OH)_{n\,(s)}$ → sludge ……(8)

In case of Al, species such as Al^{3+} and $Al(OH)_2^+$ dominate at low pH. Within the pH range 4 - 9, various species such as $Al(OH)_2^+$, $Al(OH)_2^{2+}$, which are monomeric and species such as $Al_6(OH)_{15}^{3+}$, $Al_7(OH)_{17}^{4+}$, $Al_{13}(OH)_{34}^{5+}$ which are polymeric form flocs $Al(OH)_3(s)$ through complex polymerization and/or precipitation mechanism. When pH is higher than 8, the monomeric $Al(OH)_4^-$ concentration increases, decreasing the significance of insoluble amorphous $Al(OH)_3(s)$ flocs (Merzouk et al, 2010). In case of iron electrodes, only soluble Fe^{2+} ions and Fe^{3+} (aq) ions form the precipitation of $Fe(OH)_3$ with impurities mainly by charge neutralization or adsorption during coagulation.(Cerqueira, 2009)

Direct red 81 was successfully removed by adsorption (Aoudj et al, 2010). It was observed during analysis of dye-loaded sludge using FTIR. The observed variations in FTIR spectrum suggest the adsorption of dye on $Al(OH)_3(s)$ flocs.

Some authors emphasized the importance of flotation at EC process (Ghanbari et al, 2014). The sacrificial electrode is electrolytically oxidized and coagulants are formed during an EC process. Such coagulants destabilize the contaminants and consequently agglomerates are formed. As gases are formed according to Eq. 4, pollutants are floated. The process is shown in Fig.1 as one of the main stages involved in EC processes.

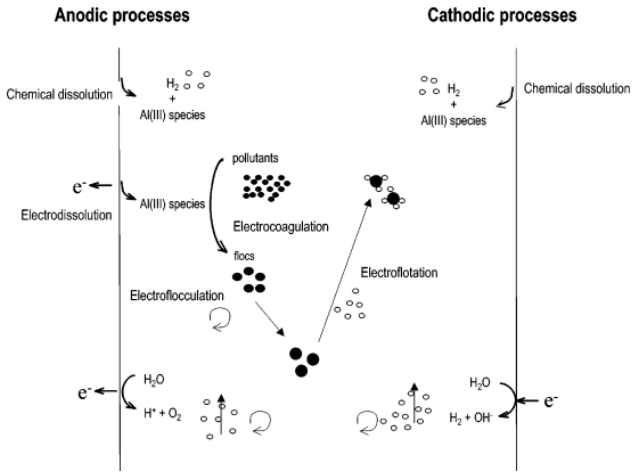

Figure 1: Main mechanism of electrocoagulation
Source: (Canizares et al., 2005)

During EC flocs are formed similar to conventional coagulation. Coloids are neutralised by Al (or Fe) ions and they generate bigger macroflocs which are removed by sedimentation. The stability of colloidal particles is well described by DLVO (Derjaguin-Landua- Verwey-Overbeek) (Moussa et al, 2017). Two forces: attractive van der Waals force with an attraction energy (V_A) and the repulsive electrostatic force with repulsion energy (V_R) are the main forces have the leading role if electrical double-layer is present at particles' surfaces (Fig .2). Around a negative ion an excess of positive ion is accumulated in the interfacial region, and this govern the electrostatic effects. If we sum the Van der Waals attraction energy and electrostatic repulsion energy we gain the net interaction energy of two particles. The total interaction curve ($V_A + V_R$) shows a primary minimum and a secondary minimum in Fig. 2.

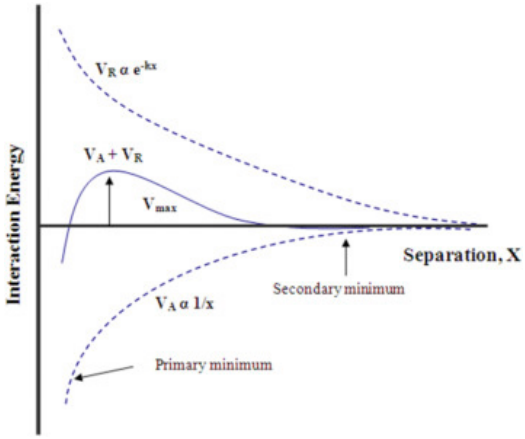

Figure 2: Interaction energy and particle separation curve in dependence of X
Source: (Moussa, 2017)

In general, laboratory EC system consist of 2 electrodes in reactor and are connected to DC source. (Mollah et al 2004).. The research related to the use of electrode made of composite of aluminum and iron which are most widely used electrode material. They both are very concise for the treatment of textile wastewater (Verma, 2017).
For real wastewater treatment a cell with two-electrode EC is not appropriate. Large surface area is required. EC cells with monopolar electrodes either in parallel or series connections could improve the efficiency of EC. This arrangement of monopolar electrodes with cells in series is electrically like a single cell. The pair of

»bipolar« electrodes are placed between the two parallel monopolar electrodes and are electrical not connected, there is no interconnections between the anodes. Only the two monopolar electrodes are connected to the electric power source. (Moussa et al, 2017)

3 Effect of important parameters on electrocoagulation efficincy

Since dying is very important branch of industry in developing countries, simple and cost-effective treatment methods are searched for effluent wastewater treatment. EC have potentials for effective method. Authors claim that the most influential factors on removal efficiency are as follows: time of EC, conductivity, pH-value, selected dye concentration, current density, and current on electrodes, which could be periodically reversal (Hakizimana et al, 2017).

3.1 Initial pH value and Conductivity

Neutral pH range was suitable in many experiments, generally at pH 7.0 ±0.5. If pH of the dye solutions was between 5.5 and 8.5 almost total colour removal was observed (Daneshvar et al, 2006) and between 6.5 and 10.5 for cationic dye removal (Nandi and Patel, 2017). Initial pH was 7.4 and 70 % of suspended solids was achieved, 97 % of Cr removal and 46 % of COD removal (Apaydin et al, 2009). Best removal results for 5 min electrolysis duration were observed at a pH of 5–9 during the EC process. (Sangil and Ozacar, 2009)and 98 % of reactive dye was degraded. Recent study showed up to 95 % colour removal at pH = 5 and current density 25 mA/cm^2 (Bener et al., 2019)

The amount of $Al(OH)_3$ overcomes the amount of OH^-, then more precipitation will be formed, causing more removal efficiency. (Khoran and Falach, 2018).

The removal of COD and colour from synthetic textile wastewater was studied (Verma, 2014): Up to 86 % colour was removed up to pH=8.

In tannery wastewater the initial pH is around 4 and slightly increases during EC. Up to 85 % of COD could be removed in acid region (Varank et al, 2014).

It could be concluded that pH has great influence on dye removal while the COD removal efficiency was lower, thus, depending on more than one parameter.
Low energy consumption was observed in another study with high Cl-ions content (Nandi Patel). The same study on removal of Brilliant green, which is very well-known cationic dye, showed the influence of NaCl. Dye diffusion and adsorption onto fibre is ehhanced by NaCl, whereas Na_2CO_3 is less efficient in dye removal at EC, which is connected to the pH increase.

Almost total colour removal can be obtained in dye solutions with a conductivity of 8 mS/cm. (Daneshvar et al, 2006)

3.2 Reaction time

If reaction time increased 6-fold from 10 min yield in the dye removal increased to 98.3 % (Aoudj et al., 2010). Electrocoagulation time was studied at 7.5 initial pH, 4.0 cm internal electrode distance, and 68 mA cm^{-2} current density values. Turbidity was lowered up to 99 %; TSS up to 60 % and Ca-ions up to 80 % in 45 min EC. (Espinoza et al, 2009) Already after 3 min COD decreased by 84 % to 78.5 mg/l with a removal efficiency of when using two iron electrodes with fixed potential of 0.6 V (Zaroual, 2006).

3.3 Current density

The optimum current density of 80 A/m^2 was used for the colour decrease if dye solution containing BB3 was treated.(Daneshvar et al, 2006) Similar values from 80 to 100 A/m^2 were reported by Kobya (Kobya et al, 2003).The optimum current density of 75 A/m^2 was applied for achieving the highest decolourisation of textile wastewater (Ghanbari, 2014).For current density up to 138.9 A/m^2, more than 90 % brilliant green dye removal was observed after 10 min of operation (Nandi and Patel, 2017). The rate of dye removal increased with increasing of current density. In another study much lower density at 19 A/m^2 was used and 98 % of dye removal was achieved. (Aoudj et al, 2010)

3.4 Initial dye concentration

The dye concentration is removed by the sufficiency of Fe species. The lower is the dye concentration better would be the removal efficiency. (Zaroual et al, 2006) The same observation was found by Auodj (Aroudi et al, 2010). If dye concentration is high less adsorption sites are available for dye to adsorb.

In general, using a steel anode, the dye decayed in the order: reactive > acid > disperse, and using Al, the order is: acid > reactive > disperse (Garcia-Segura).[22]

3.5 Electrode distance

The interelectrode distance affect differ regarding pollutant nature, hydrodynamic conditions, etc. Best efficiencies were gained at 1.5 cm at 98 % (Aoudj et al, 2010). At such distance, the most of aluminium polymers aggregate in flocs and the dye adsorption was the highest. (Ghanbari et al, 2014). The highest decolorization efficiency was achieved with a distance of 3 cm between the two anodes. At larger distances the flocs interactions are weaker, and the adsorption decreased.

The issue of cathodic polarization also discussed (Wellner et al, 2018) and the results was accumulation of $Al(OH)_4^-$ at the electrode surface.

3.6 Unit energy demand

The operating costs of EC could be calculated as a sum of the cost of energy, electrode and chemical consumption (Khandegar and Saroha, 2013).

The energy demand for certain dye removal was studied. For 75 % of dye removal the energy demand was 4.7 kWh per kg while it increased to 7.5 kWh per kg if 98 % of dye was removed (Daneshvar et al, 2006) Even lower energy consumption was determined at 0.018 kWh per kg of dye removed (Verma, 2017). 0,59 kWh per kg of dye was needed to achieve colour removal 98 % in textile wastewaters (Ghanbari, 2014) if we assume inlet dye concentration 100 mg L^{-1} of textile wastewater.

The operation of a continuous photovoltaic electrocoagulation process (PVEC) was investigated, where the photovoltaic module was used instead of the current supply (Khemila, 2018). More than 16 kWh per kg of removed dye were consumed, which was more than by using current supply.

The specific energy demand in relation for aluminium and iron electrodes was studies (Kobya et al, 2003). Iron electrodes are more energetically efficient than aluminium between pH 5 and 9. The energy consumption was 0.65 kWh/kg COD for iron electrodes, while around 0.8 kWh/kg COD for Al electrodes in acidic medium. In basic mediums costs were twice higher for both types of electrodes.
It has been reported that electrocoagulation drastically reduces the costc for the treatment of textile wastewater in comparison with coagulation (Bayramoglu et al, 2007).

4 Conclusion

The industrial potential of electrocoagulation application in textile sector for wastewater treatment was reviewed. The most influential factors were presented and discussed. The pH of the solution is one of the most important operational parameters in EC. As presented in this paper many studies on synthetic textile wastewater were performed using EC as method for COD, dyes, and colour removal. EC seemed to be an efficient process to treat textile wastewater. However, industrial scale up is more difficult as it might seem. Further work is needed to improve the stability of the process especially regarding real textile wastewater treatment, the role of hydrogen gas.

Acknowledgments

The authors acknowledge financial support from the Slovenian Research Agency (Research Programme P2-0414).

References

Moussa D.T., M.H. El-Naas, M. Nasser, M.J. Al-Marri: A comprehensive review of electrocoagulation for water treatment: Potentials and chalanges, Journal of Environmental Management 186 (2017) 1, 24-41.

Emamjomeh M. M., M. Sivakumar: Review Review of pollutants removed by electrocoagulation and electrocoagulation/flotation processes, J. Environ Manage 90 (2009) 1663-1679.

Espinoza-Quiñones F.R., M.M.T. Fornari, A.N. Módenes, S.M. Palácio, F.G. da Silva Jr., N. Szymanski, A.D. Kroumov, D.E.G. Trigueros: Pollutant removal from tannery effluent by electrocoagulation, Chemical Engineering Journal 151 (2009), 1-3, 59-65

Chen G.: Electrochemical technologies in wastewater treatment, Separation and Purification Technology, 38 (2004) 1, 11–41

Hendaoui K., F.Ayari, I. BenRayana, R.BenAmar, F. Darragi, M. Trabelsi-Ayadi: Real indigo *dyeing* effluent decontamination using continuous *electrocoagulation* cell: Study and optimization using Response Surface Methodology, Proces Safety and Environmental Protection 116 (2018) 578-589

Nandi B.K., Patel S: Effects of operational parameters on the removal of brilliant green dye from aqueous solutions by electrocoagulation, Arabian Journal of Chemistry 10 (2017) S2961-S2968

Merzouk K., A. Madani: Using electrocoagulation/electroflotation technology to treat synthetic solution and textile wastewater, two case studies, Desalination, 250 (2010) 573-577

Cerqueira A., Russo C., Marques M.R.C: Electroflocculation for textile wastewater treatment, Brazilian Journal of Chemical Engineering 26 (2009) 659-668.

Aoudj S., A. Khelifa, N. Drouiche, M. Hecini, H. Hamitouche: Electrocoagulation process applied to wastewater containing dyes from textile industry, Chemical Engineering Processing and Process Intensification 49 (2010), 11, 1176-1182

Ghanbari E., Moradi M., Eslami A., Emamjomeh M. M.: Electrocoagulation/Flotation of Textile Wastewater with Simultaneous Application of Aluminium and Iron as Anode, Environmental Processes 1 (2014) 4, 447-457.

Cañizares P., M. Carmona, J. Lobato, F. Martínez, M. A. Rodrigo: Electrodissolution of Aluminum Electrodes in Electrocoagulation Processes, Industrial Engineering Chemical Research 44 (2005) 12, 4178-4185 (DOI: 10.1021/ie048858a)

Mollah M.Y.A., Pathak S. R., Patil P.K., Vayuvegula M., Agrawal T.S., Gomes J.A.G., Kesmez M., Cocke D.L.: Treatment of Orange II azo-dye by electrocoagulation (EC) rechnique in a continuous flow cell using sacrificial iron electrodes, Journal of Hazardous Materials 109 (2004) 1-3, 165-171.

Verma A.K.: Treatment of textile wastewaters by electrocoagulation employing Fe-Al composite electrode, Journal of Water Process Engineering 20 (2017) 168-172.

Hakizimana J. N., Gourich B.,. Chafi M,, Stiriba Y, Vial C., Drogui P., Naja J.: Electrocoagulation process in water treatment: A review of electrocoagulation modeling approaches, Desalination 404 (2007) 1-21.

Daneshvar N., A. Oladegaragoze, N. Djafarzadeh: Decolorization of basic dye solutions by electrocoagulation: an investigation of the effect of operational parameters, Journal of Hazardous Materials 129 (2006), 116-122

Apaydin Ö., U. Kurt, M. Gonullu: An investigation on the treatment of tannery wastewater by electrocoagulation, Glob. NEST J. 11 (2009), 4, 546-555

Şengil, İ.A., M. Özacar: The decolorisation of C. I. Reactive Black 5 in aqueouus solution by electrocoagulation using sacrifitial iron electrodes, Journal of Hazardous Materials 161 (2009) 2-3, 1369-1376.

Khorran A. G., Fallach N.: Treatment of textile *dyeing* factory wastewater by *electrocoagulation* with low sludge settling time: Optimization of operating parameters by RSM, Journal of Environmental Chemical Engineering 6 (2018)1, 635-642.

Varank G., H. Erkan, S. Yazýcý, A. Demir, G. Engin: Electrocoagulation of tannery wastewater using monopolar electrodes: process optimization by response surface methodology, Int. J. Environ. Res. 8 (2014), 1, 165-180

Zaroual Z., M. Azzi, N. Saib, E. Chainet: Contribution to the study of electrocoagulation mechanism in basic textile effluent, Journal of Hazardous Materials 131 (2006), 1-3, 73-78

Kobya M., Can, O.T., Bayramoglu, M.: Treatment of textile wastewaters by electrocoagulation using iron and aluminum electrodes, Journal of Hazardous Materials 100 (2003) 1–3, 163–178.

Garcia-Segura S., M.M.S.G. Eiband, J.V. de Melo, C. A. Martinez-Huitle, Electrocoagulation and advanced electrocoagulation processes: A general review about the funadamentals emerging applications and its association with other technologies, Journal of Electroanalytical Chemistry 801 (2017) 267-299.

Wellner D. B., Couperthwaite S. J., G.J. Millar: Influence of operating parameters during electrocoagulation of sodium chloride and sodium bicarbonate solutions using aluminium electrodes, Journal of Water Process Engineering 22 (2018) 13-26.

Khandegar v., Saroha A. K: Electrocoagulation for the treatment of textile industry efluent – A review, Journal of Environmental Management 128 (2013) 949-963.

Khemila B., Merzouk B., Chouder A., Zidelkhir R., Leclerc J.P, Lapicque F.: Removal of a textile dye using photovoltaic *electrocoagulation*, Sustainable Chemistry and Pharmacy, 7 (2018) 27-35

Bayramoglu M., Eyvaz M., Kobya M. Treatment of the textile wastewater by electrocoagulation: economic evaluation, Chemical Engineering Journal 128 (2007) 2-3, 155-161

Can O.T., M. Kobya, E. Demirbas, M. Bayramoglu: Treatment of the textile wastewater by combined electrocoagulation, Chemosphere, 62 (2006) 2, 181-187.

Aleboyeh A, Daneshvar N, Kasiri M.B.: Optimization of C.I. Acid Red 14 azo dye by electrocoagulation batch process with response surface methodology, Chemical Engineering and Processing 47 (2008) 5, 827–832

Bener S., Bulca O., Palas B., Tekin G., Atalay S., Ersoz G., Electrocoagulation process for the treatment of real textile wastewater: Effect of operative conditions on the organic carbon removal and kinetic study, Process Safety and Environmental protection 129 (2019) 47-54.

Sandoval M.A., Fuentes R., Thiam A.,Salazar R : Arsenic and fluoride removal by electrocoagulation process: A general review, Science of The Total Environment 753 (2021) 142108.

5TH INTERNATIONAL CONFERENCE ON TECHNOLOGIES & BUSINESS MODELS FOR CIRCULAR ECONOMY: CONFERENCE PROCEEDINGS

SANJA POTRČ, MILOŠ BOGATAJ, ZDRAVKO KRAVANJA, ZORKA NOVAK PINTARIČ (EDS.)

University of Maribor, Faculty of Chemistry and Chemical Engineering, Maribor, Slovenia
sanja.potrc@um.si, milos.bogataj@um.si, zdravko.kravanja@um.si, zorka.novak@um.si

Abstract The 5th International Conference on Technologies & Business Models for Circular Economy (TBMCE) was organized by the Faculty of Chemistry and Chemical Engineering, University of Maribor in cooperation with the Chamber of Commerce and Industry of Štajerska and SRIP- Circular Economy. The conference was held in Portorož, Slovenia, at the Grand Hotel Portorož from September 12th to September 14th, 2022. TBMCE 2022 was devoted to presentations of circular economy concepts, technologies and methodologies that contribute to the shift of business entities and society as a whole to a more responsible, circular management of resources. The conference program included a round table: Asia – factory of the world, what about the EU?, 4 panel discussions, 1 plenary and 4 keynote lectures, oral and poster presentations on the following topics: Sustainable energy, Biomass and alternative raw materials, Circular business models, Secondary raw materials and functional materials, ICT in Circular Economy, Processes and technologies. The event was under the honorary patronage of Mr. Matjaž Han, Minister of Economic Development and Technology.

Keywords: circular economy, sustainable development, processes and technologies, circular business models, research and development

University of Maribor Press

DOI https://doi.org/10.18690/um.fkkt.1.2023
ISBN 978-961-286-692-1

University of Maribor

Faculty of Chemistry and Chemical Engineering

SEPTEMBER 12TH
to
SEPTEMBER 14TH
2022

PORTOROŽ, SLOVENIA